Available online at www.sciencedirect.com
ScienceDirect
International Journal of Mechanical Sciences 49 (2007) 1289–1308
International Journal of MECHANICAL SCIENCES
www.elsevier.com/locate/ijmecsci

Substepping algorithms with stress correction for the simulation of sheet metal forming process

K.Z. Ding, Q.-H. Qin*, M. Cardew-Hall

Department of Engineering, Faculty of Engineering and Information Technology, The Australian National University, Canberra ACT O200, Australia

Received 11 February 2007; accepted 11 March 2007
Available online 24 March 2007

Abstract

The finite element analysis of the sheet metal forming process involves various nonlinearities. To predict accurately the final geometry of the sheet blank and the distribution of strain and stress and control various forming defects, such as thinning, wrinkling and springback, etc., the accurate integration of the constitutive laws over the strain path is essential. Our objective in this paper is to develop an effective and accurate stress integration scheme for the analysis of three-dimensional sheet metal forming problems. The proposed algorithm is based on the explicit "substepping" schemes incorporating with the stress correction scheme. The proposed algorithms have been implemented into ABAQUS/Explicit via User Material Subroutine (VUMAT) interface platform. The algorithms are then employed to analyze a typical deep-cup drawing process and the accuracy of these algorithms has been compared with the implicit "return" algorithm and explicit forward algorithm. The results indicate that the explicit schemes with local truncation error control, together with a subsequent check of the consistency conditions, can achieve the same or even better level of accuracy as "return" algorithm does for integrating large plastic problems like sheet metal forming process.

Keywords: Finite element analysis; Sheet metal forming; Stress integration; Nonlinear elastic–plastic problems

1. Introduction

In recent years considerable effort has been made in solving sheet metal stamping problems using the finite element method. The aim has been to minimize the time and cost for process development and production while minimizing scrap and optimizing the quality of the parts produced. Through use of finite element simulation, researchers and industrial practitioners can understand more about the forming process by predicting key outcomes of the forming process such as the final shape of the part, flow of material, possibility of failure based on necking, wrinkling and amount of springback. It is well known that the accuracy with which the constitutive models are integrated has a direct impact on the overall accuracy of the analysis. An accurate algorithm for integrating the stress–strain relations is therefore a key factor to make the analysis on extremely complicated sheet metal forming process successful.

Most commonly used stress update schemes for integration of elastic–plastic constitutive laws fall within the categories of forward (explicit) and backward (implicit) algorithms. During the past decades, implicit algorithms have drawn growing attentions for their excellent convergent performance in nonlinear analysis. Nowadays, return mapping schemes dominate implicit algorithms used in the most commercial finite element software packages such as ABAQUS, ANSYS, LS-DYNA. The first implicit return mapping algorithm developed was the radial return algorithm proposed by Wilkins [1] for the elastic–perfectly plastic Von Mises model. The algorithm was subsequently assessed by Krieg and Kreig [2]. A complete accuracy analysis of the algorithm was conducted in Ref. [3]. Implicit methods are attractive because the resulting stress states automatically satisfy the yield criterion to a specified tolerance. Furthermore, with implicit algorithm above the determination of the initial yielding state, i.e. the intersection with the yield surface, becomes unnecessary if the

*Corresponding author. Tel.: +61 2 612 58274; fax: +61 2 612 50506.
E-mail address: Qinghua.Qin@anu.edu.au (Q.-H. Qin).

0020-7403/$ - see front matter © 2007 Elsevier Ltd. All rights reserved.
doi:10.1016/j.ijmecsci.2007.03.010

stress point changes from an elastic state to a plastic state. In spite of these advantages, the usage of the algorithms has been largely restricted to simple plasticity models, such as Von Mises plasticity. However, as more and more complicated constitutive models, including non-associated flow rule, complex yield criteria and hardening laws, are being developed for simulating the sheet metal forming accurately, application of the existing implicit algorithms to sheet metal forming analysis is quite often cumbersome and the convergence is not always guaranteed.

Compared with implicit algorithms, the explicit algorithm has the advantage of being more straightforward to implement. The best-known explicit method for integrating elastic–plastic stress–strain relations is forward Euler scheme. However, this technique requires that load increments be kept small enough so that the stresses computed at the end of integration procedure do not deviate too far from the yield surface. For the applications with relative large load increments, the computed stresses may not satisfy the yield criterion after integration process. Therefore, a correction of stresses has been used frequently. A detailed introduction of the methods for correcting the stresses to the yield surface can be found in Ref. [4]. Since the number of substeps is usually determined by an empirical rule which is formulated by trial and error, the inappropriate choice of the number of the substeps usually leads to lose of either accuracy or efficiency.

A number of integration algorithms therefore were developed with the aim to control the error in the integration process. For example, Polat and Dokainish [5] used an automatic subincrementation scheme for accurate integration of elastic–plastic constitutive relations. Wissmann and Hauck [6] introduced an algorithm into the integration process by using Richardson extrapolation to select a number of fixed size substeps. Pezeshk and Camp [7] suggested that an integration method based on a Modified Trapezoidal Rule Method may be simple and effective. It is especially worthy noting that two explicit schemes with adaptive substepping developed by Sloan [8,9], the modified Euler scheme and the Runge–Kutta–England scheme, in which the difference between the solutions obtained via two integration procedures with truncation errors of different order is used to determine the substep size. This idea has been further adopted and extended in a series of papers by Luccioni et al. [10], Tamagnini et al. [11], Jakobsen and Lade [12] and Fellin and Ostermann [13]. However, very few studies have been conducted in terms of comparing the substepping schemes with implicit schemes. The work of Tamagnini et al. [11] and Potts and Ganendra [14] made some progress in this field. The numerical results in both works above indicated that the substepping schemes are more robust and efficient than the implicit schemes. However, it has been found that most of the existing works in this area focused on the plasticity in geomechanics. To the authors' knowledge, the plasticity that occurs in geo-materials such as clay is very small due to their limitation to tolerate the plastic deformation. Also, as pointed out in Ref. [11], the use of "*simple*" numerical models, for example in Ref. [14], and reference to a given boundary value problem, rather than at the integration point level, made such comparisons not applicable for large plastic deformation problems. Gens and Potts [15] studied these two substepping schemes and suggested that the deviation from the yield surface is directly related to the level of error in computed stresses and it is practically independent of the integration scheme adopted. Crisfield [16] also strongly advocates some form of stress correction when the model involves the hardening, as the drift is found to be generally more pronounced. Since such discrepancies are usually cumulative, it is important to ensure that the stresses are corrected back to the yield surface at any time. As will be shown in Section 4, the substepping schemes with the error control are not satisfactory without correcting yield surface drift. However, they are superior to the implicit schemes when the convergence tolerance is adequate small and some form of the stress correction is applied at the end of step.

Through presenting this paper, the performance of the implicit and explicit schemes with stress correction is investigated by conducting an elastic–plastic analysis of a typical three-dimensional sheet metal forming process. An outline of the paper is as follows. Section 2 presents a fundamental elastic–plastic stress–strain formulation used in the elastic–plastic finite element computations. In Section 3, the proposed integration schemes, including radial return scheme, modified Euler scheme and Runge–Kutta–Dormand–Prince scheme, incorporating with stress correction approaches, are described in detail. Numerical experiments are reported in Section 4 and concluding remarks are offered in Section 5.

2. Fundamental elastic–plastic formulation

The general constitutive rule was introduced based on the theory of elastic–plasticity with an isotropic hardening [17]. Starting from the assumption that the total strain increment may be additively decomposed into an elastic and a plastic part, $\Delta\varepsilon_e$ and $\Delta\varepsilon_p$, respectively

$$\Delta\varepsilon = \Delta\varepsilon_e + \Delta\varepsilon_p, \tag{1}$$

where the elastic strain increments are related to stress increments by a symmetric matrix of constants D_e as

$$\Delta\varepsilon_e = D_e^{-1} : \Delta\sigma \tag{2}$$

and it is assumed that the plastic strain increment is proportional to the stress gradient of a quantity termed the *plastic potential* Q, so that

$$\Delta\varepsilon_p = \Delta\lambda \frac{\partial Q}{\partial \sigma}, \tag{3}$$

where λ is a non-negative plastic scalar. So we can rewrite Eq. (1) as

$$\Delta\varepsilon = D_e^{-1} : \Delta\sigma + \frac{\partial Q}{\partial \sigma}\Delta\lambda. \tag{4}$$

It is quite generally postulated that yielding can occur only if the stress σ satisfy the general yield criterion

$$F(\sigma, \kappa) = 0, \tag{5}$$

where κ is a hardening parameter, which is dependent on the plastic loading history. A typical hardening parameter commonly used in practice is the *effective plastic strain* $\bar{\varepsilon}_p$ defined by

$$\bar{\varepsilon}_p = \sqrt{\mathrm{d}\varepsilon_p : \mathrm{d}\varepsilon_p}. \tag{6}$$

The effective plastic strain is seen as the accumulation of plastic strain. Another commonly used hardening parameter is the *plastic work* W_p defined by

$$W_p = \sigma : \mathrm{d}\varepsilon_p. \tag{7}$$

The plastic work physically represents the energy dissipation associated with plastic deformation.

Eqs. (6) and (7) together with the flow rule of Eq. (3) indicate that the increment of the hardening parameter $\Delta\kappa$ can be expressed in general as

$$\Delta\kappa = \Delta\lambda h, \tag{8}$$

where h is a scalar function defined by

$$h = \begin{cases} \left\| \frac{\partial Q}{\partial \sigma} \right\| & \text{Strain hardening,} \\ \sigma \frac{\partial Q}{\partial \sigma} & \text{Work hardening.} \end{cases}$$

When plastic yielding is occurring the stresses are on the yield surface given by Eq. (5). Differentiating this we can therefore write

$$\mathrm{d}F = \frac{\partial F}{\partial \sigma}\Delta\sigma + \frac{\partial F}{\partial \kappa}\Delta\kappa = 0. \tag{9}$$

Eqs. (5) and (9) are known as *consistency conditions*, which must be maintained when plastic yielding occurs.

By using Eqs. (1)–(9), we obtain, after some transformation, the complete elastic–plastic incremental stress–strain relation to be

$$\Delta\sigma = (D_e - D_p) : \Delta\varepsilon = D_{ep} : \Delta\varepsilon \tag{10}$$

and

$$D_{ep} = D_e - D_e : \left\{\frac{\partial Q}{\partial \sigma}\right\} : \left\{\frac{\partial F}{\partial \sigma}\right\}^{\mathrm{T}} : D_e \left[H + \left\{\frac{\partial F}{\partial \sigma}\right\}^{\mathrm{T}} : D_e : \left\{\frac{\partial Q}{\partial \sigma}\right\} \right]^{-1}, \tag{11}$$

where H is the hardening modulus, which is generally assumed to be a function of the hardening parameter κ. For associated plasticity, which is adopted in this project, the plastic potential Q is assumed to be consistent with the yield function F. So we can simply write D_{ep} as

$$D_{ep} = D_e - \frac{D_e : a : a^{\mathrm{T}} : D_e}{H + a^{\mathrm{T}} : D_e : a}, \tag{12}$$

in which

$$a^{\mathrm{T}} = \frac{\partial F}{\partial \sigma} = \left[\frac{\partial F}{\partial \sigma_x}, \frac{\partial F}{\partial \sigma_y}, \frac{\partial F}{\partial \sigma_z}, \frac{\partial F}{\partial \tau_{xy}}, \frac{\partial F}{\partial \tau_{yz}}, \frac{\partial F}{\partial \tau_{zx}}\right], \tag{13}$$

$$H = -\frac{1}{\Delta\lambda}\frac{\partial F}{\partial \kappa}\Delta\kappa. \tag{14}$$

Usually, we write Eq. (10) in the following form which is convenient for numerical computation

$$\Delta\sigma = D_e : \Delta\varepsilon_e - \Delta\lambda D_e : a^{\mathrm{T}}, \tag{15}$$

where

$$\Delta\lambda = \frac{1}{H + a^{\mathrm{T}} : D_e : a} a^{\mathrm{T}} : D_e : \Delta\varepsilon_e. \tag{16}$$

3. Integration of the stress–strain relations

The following procedure is commonly adopted for elasto-plastic analysis. Within a particular load increment r, the strain increments $\Delta\varepsilon^r$ can be determined via the displacement increments. Once the strain have been determined, the stress increments may be calculated using Hooke's law under the assumption of elastic behavior:

$$\Delta\sigma^r_{trial} = D_e : \Delta\varepsilon^r \tag{17}$$

and a trial stress state is obtained through

$$\sigma^r_{trial} = \sigma^{r-1} + \Delta\sigma^r_{trial}. \tag{18}$$

The trial stress σ^r_{trial} is then tested in Eq. (5). If $F(\sigma^r_{trial}, \kappa^{r-1}) \leqslant 0$, then the elasticity assumption is taken to be valid, and σ^r_{trial} is considered as the new stress state. If $F(\sigma^r_{trial}, \kappa^{r-1}) > 0$, the plastic yielding occurs. In this case, the final stress state needs to be determined by integrating the stress–strain relations over the strain path. The integration of stress–strain relations requires the solution of the initial value problem like

$$\frac{\mathrm{d}\sigma}{\mathrm{d}T} = D_{ep}\Delta\varepsilon, \quad T \in [0, 1], \tag{19}$$

in which $\sigma|_{T=0}$ defines the stress state which already satisfies the yield criterion, and $\sigma|_{T=1}$ defines the stress at an end of load increment or iteration.

Integrating the constitutive relations to obtain the unknown increment of the stresses is a key step in nonlinear elastic–plastic finite element analysis. The methods commonly used at the present are usually classified as explicit or implicit. In an explicit integration scheme, the yield surface, plastic gradients and hardening parameter are all evaluated based on known stress states of last substep. In a fully implicit method, all the internal variables are evaluated at unknown stress states of the current substep, resulting a system of nonlinear equations

must be solved iteratively. In the following, both implicit and explicit schemes are introduced in detail.

3.1. Implicit return algorithm

Implicit methods are attractive because the consistency condition is automatically satisfied at the end of integration. Furthermore, they do not require to determine the initial yielding point if the plastic yielding occurs at the stress point. A comprehensive discussion of various implicit integration schemes for elastic–plastic models can be found in Ortiz and Simo [3], Crisfield [16] and Belytschko et al. [18]. One of the most popular of these is the backward Euler algorithm which is based on the concept of an elastic predictor with a plastic return mapping. In its most general form, the final stresses and hardening parameters are found by solving a small system of nonlinear equations at each Gauss point iteratively. Although most recent work preferred to use the backward Euler scheme, it is difficult to implement such procedure for complex constitutive relations since it requires second-order derivatives of the yield function and plastic potential. Moreover, for yield surfaces with vertices or rapid changes in curvature, divergence may occur and it is advisable to use multi-vector return schemes [16].

Having the set $(\varepsilon_n, \varepsilon_n^p, \kappa_n)$ at time n and the strain increment $\Delta\varepsilon$, the plastic strain increment at time $n+1$ is given by

$$\Delta\varepsilon_{n+1}^p = \varepsilon_{n+1}^p - \varepsilon_n^p = \Delta\lambda_{n+1} r_{n+1}. \tag{20}$$

Thus, we obtain

$$\begin{aligned}\sigma_{n+1} &= D_e : (\varepsilon_{n+1} - \varepsilon_n^p - \Delta\varepsilon_{n+1}^p)\\ &= D_e : (\varepsilon_n + \Delta\varepsilon - \varepsilon_n^p - \Delta\varepsilon_{n+1}^p)\\ &= D_e : (\varepsilon_n - \varepsilon_n^p) + D_e : \Delta\varepsilon - D_e : \Delta\varepsilon_{n+1}^p\\ &= (\sigma_n + D_e : \Delta\varepsilon) - D_e : \Delta\varepsilon_{n+1}^p\\ &= \sigma_{n+1}^{trial} - D_e : \Delta\varepsilon_{n+1}^p\\ &= \sigma_{n+1}^{trial} - \Delta\lambda_{n+1} D_e : r_{n+1},\end{aligned} \tag{21}$$

where $\sigma_{n+1}^{trial} = \sigma_n + D_e : \Delta\varepsilon$ is the *trial stress of elastic predictor* and the quantity $-\Delta\lambda_{n+1} D_e : r_{n+1}$ is the *plastic corrector* which returns or projects the trial stress onto the suitable updated yield surface along a direction specified by the plastic flow direction at the end-point. The elastic-predictor phase is driven by the increment in total strain while the plastic-corrector phase is driven by the increment $\Delta\lambda_{n+1}$ in the plasticity parameter. During the plastic-corrector stage, the total strain is fixed. Thus, we have, during the plastic-corrector phase,

$$\Delta\sigma_{n+1} = -D_e : \Delta\varepsilon_{n+1}^p = -\Delta\lambda_{n+1} D_e : r_{n+1}. \tag{22}$$

The solution of the set of nonlinear algebraic equations is typically obtained by a Newton procedure. We write the plastic updates and yield condition in the form suitable for Newton iteration:

$$\begin{aligned}a &= \varepsilon^p + \varepsilon_n^p + \Delta\lambda r = 0,\\ b &= -\kappa + \kappa_n + \Delta\lambda h = 0,\\ F &= F(\sigma,\kappa) = 0.\end{aligned} \tag{23}$$

Linearization of these equations at iteration k gives (using (22) in the form $\Delta\varepsilon^{p(k)} = -D_e^{-1} : \Delta\sigma^{(k)}$)

$$\begin{aligned}&a^{(k)} + D_e : \Delta\sigma^{(k)} + \Delta\lambda^{(k)}\Delta r^{(k)} + \delta\lambda^{(k)} r^{(k)} = 0,\\ &b^{(k)} - \Delta\kappa^{(k)}\Delta\lambda^{(k)}\Delta h^{(k)} + \delta\lambda^{(k)} h^{(k)} = 0,\\ &F^{(k)} = F_\sigma^{(k)} : \Delta\sigma^{(k)} + F_\kappa^{(k)} \cdot \Delta\kappa^{(k)} = 0,\end{aligned} \tag{24}$$

where

$$\begin{aligned}\Delta r^{(k)} &= r_\sigma^{(k)} : \Delta\sigma^{(k)} + r_\kappa^{(k)} : \Delta\kappa^{(k)},\\ \Delta h^{(k)} &= h_\sigma^{(k)} : \Delta\sigma^{(k)} + h_\kappa^{(k)} \cdot \Delta\kappa^{(k)},\end{aligned} \tag{25}$$

and where a subscript σ or κ denotes a partial derivative. Eqs. (24) are a set of three equations which can be solved for $\Delta\sigma^{(k)}$, $\Delta\kappa^{(k)}$ and $\delta\lambda^{(k)}$. Substituting (25) into the first two of (24) and writing the resulting pair of equations in matrix form gives

$$[A^{(k)}]^{-1}\begin{Bmatrix}\Delta\sigma^{(k)}\\ \Delta\kappa^{(k)}\end{Bmatrix} = -\{\tilde{b}^{(k)}\} - \delta\lambda^{(k)}\{\tilde{a}^{(k)}\}, \tag{26}$$

where

$$[A^{(k)}]^{-1} = \begin{bmatrix} D_e^{-1} + \Delta\lambda a_\sigma & \Delta\lambda a_\kappa \\ \Delta\lambda h_\sigma & -I + \Delta\lambda h_\kappa \end{bmatrix}^{(k)},$$

$$\{\tilde{b}^{(k)}\} = \begin{Bmatrix} a^{(k)} \\ b^{(k)} \end{Bmatrix},$$

$$\{\tilde{a}^{(k)}\} = \begin{Bmatrix} r^{(k)} \\ h^{(k)} \end{Bmatrix}.$$

Solving (26) for the stress and internal variable increments gives

$$\begin{Bmatrix}\Delta\sigma^{(k)}\\ \Delta\kappa^{(k)}\end{Bmatrix} = -[A^{(k)}]\{\tilde{a}^{(k)}\} - \delta\lambda^{(k)}[A^{(k)}]\{\tilde{r}^{(k)}\}. \tag{27}$$

Substituting this result into (24) and solving for $\delta\lambda^{(k)}$ we get

$$\delta\lambda^{(k)} = \frac{F^{(k)} - \partial F^{(k)} A^{(k)} \tilde{a}^{(k)}}{\partial F^{(k)} A^{(k)} \tilde{r}^{(k)}}. \tag{28}$$

Thus, the update of the plastic strain, internal variables and the plasticity parameter is

$$\begin{aligned}\varepsilon^{p(k+1)} &= \varepsilon^{p(k)} + \Delta\varepsilon^{p(k)} = \varepsilon^{p(k)} - D_e^{-1} : \Delta\sigma^{(k)},\\ \kappa^{(k+1)} &= \kappa^{(k)} + \Delta\kappa^{(k)},\\ \Delta\lambda^{(k+1)} &= \Delta\lambda^{(k)} + \delta\lambda^{(k)}\end{aligned}$$

with the increments as given in (27) and (28). The Newton procedure is continued until convergence to the updated yield surface is achieved to within a sufficient tolerance. The complete backward Euler algorithm is given in Table 1.

Table 1
Backward Euler return mapping algorithm

1. Initialization: set initial values of plastic strain and internal variables to converged values at end of previous time-step, zero the increment in plasticity parameter and evaluate the elastic trial stress:
$k=0, \quad \varepsilon^{p(0)}=\varepsilon_n^p, \quad \kappa^{(0)}=\kappa_n, \quad \Delta\lambda^{(0)}=0, \quad \sigma^{(0)}=D_e:(\varepsilon_{n+1}-\varepsilon^{p(0)})$

2. Check yield condition and convergence at kth iterations:
$F^{(k)}=F(\Delta\sigma^{(k)},\Delta\kappa^{(k)}), \quad \{\tilde{a}^{(k)}\}=\begin{Bmatrix} a^{(k)} \\ b^{(k)} \end{Bmatrix}$

If: $F^{(k)}<TOL_1$ and $\|\tilde{a}^{(k)}\|<TOL_2$, converged.
Else: go to 3.

3. Compute increment in plasticity parameter:
$[A^{(k)}]^{-1}=\begin{bmatrix} D_e^{-1}+\Delta\lambda r_\sigma & \Delta\lambda r_\kappa \\ \Delta\lambda h_\sigma & -I+\Delta\lambda h_\kappa \end{bmatrix}^{(k)}, \quad \{\tilde{r}^{(k)}\}=\begin{Bmatrix} r^{(k)} \\ h^{(k)} \end{Bmatrix}, \quad \partial F=[F_\sigma \; F_\kappa]$

$\delta\lambda^{(k)}=\dfrac{F^{(k)}-\partial F^{(k)}A^{(k)}\tilde{b}^{(k)}}{\partial F^{(k)}A^{(k)}\tilde{a}^{(k)}}$

4. Obtain increments in stress and internal variables:
$\{\Delta\sigma^{(k)}\Delta\kappa^{(k)}\}=-[A^{(k)}]\{\tilde{a}^{(k)}\}-\delta\lambda^{(k)}[A^{(k)}]\{\tilde{r}^{(k)}\}$

5. Update plastic strain and internal variables:
$\varepsilon^{p(k+1)}=\varepsilon^{p(k)}+\Delta\varepsilon^{p(k)}=\varepsilon^{p(k)}-D_e^{-1}:\Delta\sigma^{(k)}$

$\kappa^{(k+1)}=\kappa^{(k)}+\Delta\kappa^{(k)}$

$\Delta\lambda^{(k+1)}=\Delta\lambda^{(k)}+\delta\lambda^{(k)}$

$\sigma^{(k+1)}=\sigma^{(k)}+\Delta\sigma^{(k)}=D_e:(\varepsilon_{n+1}-\varepsilon^{p(k+1)})$

$k<-k+1$, go to 2

3.2. Explicit integration schemes

Compared with implicit methods, explicit methods can be used to implement a general integration for any elastic–plastic models as it only needs first derivative of the yield function and plastic potential. However, to achieve a better accuracy of the integration, the strain increment that constitutes an elastic–plastic response is usually divided into a number of substeps. Since the determination of the number of substeps are completely based on trial and error and there is no error control in the whole integration process, some forms of the stress correction are often used to return the stress state to the yield surface. For this purpose, Wissmann and Hauck [6] and Sloan [8] suggested a substepping scheme with error control to limit the error accumulation in the computed stresses. However, as shown in the next section, such schemes only provide the desirable accuracy when used in conjunction with the stress correction. For all the explicit schemes, the initial yielding point is needed for the integration process to start with. In the following, the methods for restoring the stress states to the yield surface and determining the intersection point are introduced.

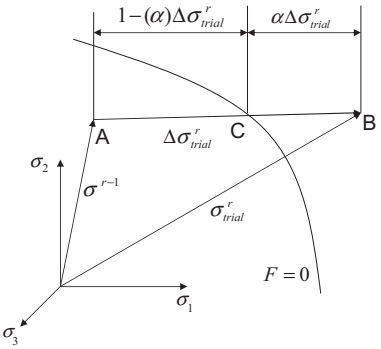

Fig. 1. Schematic illustration of the initial yielding state.

3.2.1. Intersection with the yield surface

As mentioned previously, if $F(\sigma^{(r-1)},\kappa^{(r-1)})<0$ and $F(\sigma_{trial},\kappa^{(r-1)})>0$, the plastic yielding occurs during this increment and the strain increment is partly in an elastic path and partly in a plastic path. Assume that the stress state changes from last elastic state σ^{r-1} (point A) to an elastic–plastic state (point B) shown in Fig. 1. In order to determine the portion of the stress which cause purely plastic yielding, we need to find a scalar α such

that

$$F(\sigma^r, \kappa^{(r-1)}) = 0,$$

where

$$\sigma^r = \sigma^{r-1} + (1-\alpha)\Delta\sigma_{trial}$$

to ensure that the stress state at point C lies on the yield surface. A variety of schemes are available for determining scalar α. A simple linear interpolation method used in Ref. [17] gives:

$$\alpha = -\frac{F(\sigma^{(r-1)})}{F(\sigma_{trial}) - F(\sigma^{(r-1)})}. \tag{29}$$

Sloan [8] used a Newton–Raphson iteration to compute α. In this paper, an iterative scheme is used with the aim to maintain sufficient accuracy for the plasticity integration. The intersection point, i.e. α may be obtained by iteratively solving

$$\sigma_k = \sigma_{k-1} + \alpha_k \Delta\sigma_{trial}, \tag{30}$$

$$\alpha_{k+1} = \alpha_k + \Delta\alpha_{k+1}, \tag{31}$$

in which

$$\Delta\alpha_{k+1} = \frac{-F(\sigma_k, \kappa)}{a_k^{\mathrm{T}} \Delta\sigma} \tag{32}$$

with the starting point at $\sigma_0 = \sigma^{r-1}$ and use the value in Eq. (29) for α_1. After determining the initial plastic yielding, we must reduce the excess stress onto the yield surface to maintain the consistency condition.

3.2.2. Correction of the yield surface drift

If the explicit integration schemes are used for updating the stress, the stress state at the end of the increment may not fulfill the yield criterion. The error will essentially depend on the size of the strain increment and number of subdivisions, but as the error is cumulative it is important to ensure that the stresses are corrected back to the yield surface during each increment. Among the five methods of projecting back in Ref. [4], the method called "projecting back along the plastic flow direction" has been proved to be the best one and will be used in this project.

The schematic illustration of the correcting process is shown in Fig. 2. Assume that the initial stress state (point A) locates on the yield surface, i.e. $F(\sigma_A, \kappa_A) = 0$ and the new stress state after integration (point B) drifts away from the updated yield surface $F(\sigma_B, \kappa_B) = 0$. The point C represents the stress state after correction. Due to the nature of the plastic flow direction normal to the yield surface for Von Mises plasticity, we have:

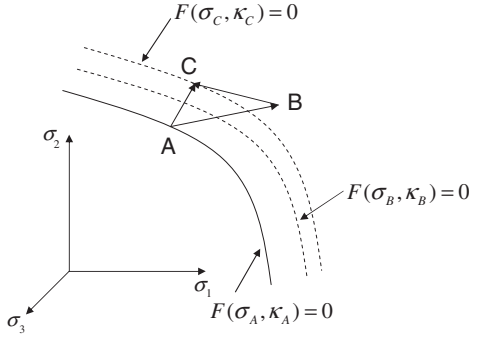

Fig. 2. Schematic illustration of the stress correction process.

$$\sigma_C = \sigma_B - \beta\frac{\partial F}{\partial \sigma}, \tag{33}$$

where β is a scalar quantity. Since the hardening parameter remains unchanged, we have the updated yield condition as

$$F(\sigma_C, \kappa_C) = F\left(\left(\sigma_B - \beta\frac{\partial F}{\partial \sigma}\right), \kappa_B\right) = 0. \tag{34}$$

The updated scalar β can be obtained by a Taylor series expansion:

$$\beta = \frac{F(\sigma_B, \kappa_B)}{(\partial F/\partial\sigma)(\partial F/\partial\sigma)^{\mathrm{T}}} \tag{35}$$

$$= \frac{F(\sigma_B, \kappa_B)}{a : a^{\mathrm{T}}}. \tag{36}$$

If the load increment is small the above procedure just need one step to maintain the consistency condition. However, it is generally suggested to check that the yield criterion is fulfilled to some tight tolerance after correction. If this is not the case, an iterative procedure is then necessary with the starting point of $\sigma_0 = \sigma_b$ and $\kappa_0 = \kappa_b$.

3.2.3. Forward Euler method

The explicit forward Euler scheme is based on the intersection point in the stress and hardening parameter space for finding all the relevant derivatives and variables. To this end, the stresses are updated by replacing the infinitesimal elastic–plastic stress–strain relation by a finite incremental relation:

$$\Delta\sigma = D_{ep}(\sigma_0, \kappa_0)\Delta\varepsilon, \tag{37}$$

where the initial elastic–plastic constitutive matrix is evaluated at the intersection point. Obviously this linear approximation will not be accurate for very large strain increments. Thus, the strain increment is usually divided into smaller subincrements [19]:

$$\delta\varepsilon = \frac{(1-\alpha)\Delta\varepsilon}{m}, \tag{38}$$

where m is the number of the substeps. The changes of the stress and hardening parameter for each substep are determined as

$$\delta\sigma_i = D_{ep}(\sigma + \delta\sigma_{i-1}, \kappa + \delta\kappa_{i-1})\delta\varepsilon,$$
$$\delta\kappa_i = \delta\lambda(\sigma + \delta\sigma_{i-1}, \kappa + \delta\kappa_{i-1}, \delta\varepsilon)h,$$

where the stress and hardening parameter are updated as the sum of $\delta\sigma_i$ as the substep proceeds

$$\sigma = \sigma_0 + \sum \delta\sigma_i,$$
$$\kappa = \kappa_0 + \sum \delta\kappa_i.$$

Table 2
Forward Euler scheme with subincrements

1.	Set the initial state to be the state on intersection point: $\sigma = \sigma_0, \quad \kappa = \kappa_0, \quad \Delta\varepsilon$
2.	Determine the size of substep: $\delta\varepsilon = \frac{\Delta\varepsilon}{m}$
3.	Do at each substep, i.e. $i = 1, 2, \ldots, m$: $\delta\sigma_i = D_{ep}(\sigma_{i-1}, \kappa_{i-1})\delta\varepsilon$
	$\delta\kappa_i = \delta\lambda(\sigma_{i-1}, \kappa_{i-1}, \delta\varepsilon)h_{i-1}$
	$\sigma_i = \sigma_{i-1} + \delta\sigma_i$
	$\kappa_i = \kappa_{i-1} + \delta\kappa_i$
	Stop incrementation when $i > m$
4.	Update the stress state $\sigma = \sigma_i, \quad \kappa = \kappa_i$

The forward Euler scheme, as illustrated in Table 2, is the easiest to implement among all the explicit schemes. However, the stress states after integration tend to drift away from the yield surface if the number of the substeps is not sufficient small. Such a departure of stress from the yield surface is accumulative, and may lead to unacceptable solution for the whole load increment. Moreover, the procedure always uses subincrements of equal size, which turns out to be computationally inefficient as the number of substeps is always determined by trial and error.

3.2.4. Modified Euler method

The modified Euler scheme with active error control was introduced in Sloan [8] and Jakobsen and Lade [12] with the aims to reduce yield surface drift and computational costs of the forward Euler scheme. Instead of using a constant substep size, this explicit scheme uses the difference between the solutions obtained with two embedded Euler algorithms of different order of accuracy to extrapolate the substep size which can achieve a prescribed accuracy of the solution.

By defining a dimensionless time T such that $T \in (0, 1)$, the strain increment for a substep k is given by

$$\delta\varepsilon^{(k)} = \Delta T^{(k)}\Delta\varepsilon. \tag{39}$$

The first estimate of the updated stress and the hardening parameter at the end of the substep is given by

$$\sigma = \sigma_0 + \delta\sigma_1, \tag{40}$$

$$\kappa = \kappa_0 + \delta\kappa_1, \tag{41}$$

where

$$\delta\sigma_1 = D_{ep}(\sigma_0, \kappa_0)\delta\varepsilon^{(k)},$$
$$\delta\kappa_1 = \delta\lambda(\sigma_0, \kappa_0, \delta\varepsilon^{(k)})h^{(k)}.$$

A more accurate estimate of the updated stress may be found by using second-order Euler algorithm:

$$\hat{\sigma} = \sigma_0 + (\delta\sigma_1 + \delta\sigma_2)/2,$$
$$\hat{\kappa} = \kappa_0 + (\delta\kappa_1 + \delta\kappa_2)/2,$$

where

$$\delta\sigma_2 = D_{ep}(\sigma_0 + \delta\sigma_1, \kappa_0 + \delta\kappa_1)\delta\varepsilon^{(k)},$$
$$\delta\kappa_2 = \delta\lambda(\sigma_0 + \delta\sigma_1, \kappa_0 + \delta\kappa_1, \delta\varepsilon^{(k)})h^{(k)}.$$

Based on the two solutions available, an estimate of the local error in σ can be given by

$$E = \hat{\sigma} - \sigma = (\delta\sigma_2 - \delta\sigma_1)/2. \tag{42}$$

This error estimate serves as a guide for selecting the size of the next time step, ΔT, when integrating over the total strain increment $\Delta\varepsilon$. That is, the relative error for this substep is defined by

$$R^{(k)} = \|\hat{\sigma} - \sigma\|/\|\hat{\sigma}\|. \tag{43}$$

Then R is compared with some prescribed tolerance TOL and the step is accepted if $R \leqslant TOL$, and rejected otherwise. Furthermore, the value of R allows us to make an estimate for the asymptotically optimal substep size:

$$\Delta T^{(k+1)} = \Delta T^{(k)}\sqrt{TOL/R}.$$

In case of rejection $\Delta T^{(k+1)}$ is used instead of $\Delta T^{(k)}$; in case of acceptance we use $\Delta T^{(k+1)}$ to continue the integration. The modified Euler algorithm, which incorporates error control and a variable step size for each integration point, may be summarized as in Table 3.

As shown in Table 3, in order to serves to prevent an abrupt change in the substep size. In our subroutine, we actually implemented

$$\Delta T^{(k+1)} = \Delta T^{(k)} \cdot min\left\{2, max\left\{0.1, 0.9\sqrt{TOL/R^{(k)}}\right\}\right\} \tag{44}$$

and the safety factor 0.9 is added to increase the probability that next substep will be accepted [20]. By controlling the local relative error for each substep, this scheme aims to control the global relative error in the overall solution.

3.2.5. Runge–Kutta–Dormand–Prince integration scheme

Runge–Kutta type schemes are widely used for stress integration purpose due to their high order of accuracy. One algorithm which have been successfully used in elastic–plastic computations [9,12] is the Runge–Kutta–Dormand–Prince (RKDP) method, introduced by Dormand and Prince [21]. One of its advantages is that high-order estimate, $\hat{\sigma}$, for the solution can be obtained without any extra function evaluations. Runge–Kutta–Dormand–Prince is a seven-stage scheme, but effectively uses only six function evaluations. Different from the coefficients used in Refs. [9,12], the coefficients of the Runge–Kutta–Dormand–Prince shown in Fig. 3 is chosen based on the

Table 3
Modified Euler scheme with subincrements

1. Determine the initial state for σ, κ, substep counter k, time T and its increment ΔT:
   $\sigma = \sigma_0, \quad \kappa = \kappa_0, \quad k = 1, \quad T = 0, \quad \Delta T = 1$
2. While $T \leqslant 1$, perform 3 to 10. Otherwise go to 11.
3. Determine the substep size:
   $\Delta\varepsilon^{(k)} = \Delta T \Delta\varepsilon$
4. Calculate $\Delta\sigma_i$ and $\Delta\kappa_i$ for i from 1 to 2 according to:
   $\Delta\sigma_i = D_{ep}(\sigma_i, \kappa_i)\Delta\varepsilon^{(k)}$
   $\Delta\kappa_i = \Delta\lambda(\sigma_i, \kappa_i)h^{(k)}$
5. Compute approximate solutions for $\sigma^{(k)}$ and $\kappa^{(k)}$:
   $\sigma^{(k)} = \sigma^{(k-1)} + \Delta\sigma_1$
   $\kappa^{(k)} = \sigma^{(k-1)} + \Delta\kappa_1$
   $\hat{\sigma}^{(k)} = \sigma^{(k-1)} + \frac{1}{2}(\Delta\sigma_1 + \Delta\sigma_2)$
   $\hat{\kappa}^{(k)} = \kappa^{(k-1)} + \frac{1}{2}(\Delta\kappa_1 + \Delta\kappa_2)$
6. Compute the estimate of the relative error for the current substep:
   $R^{(k)} = \dfrac{\|\hat{\sigma}^{(k)} - \sigma^{(k)}\|}{\|\hat{\sigma}^{(k)}\|}$
7. Check if the current substep is accepted or rejected:
   IF $R^{(k)} > TOL$ GO TO 10
8. Update the stress, hardening parameter and integration time:
   $\sigma^{(k)} = \hat{\sigma}, \quad \kappa^{(k)} = \hat{\kappa}, \quad T = T + \Delta T$
9. Evaluate next substep size:
   $\Delta T \leftarrow \Delta T_{k+1} = \Delta T^{(k)} \cdot min\left\{0.9\left[\dfrac{TOL}{R^{(k)}}\right]^{1/2}, 2.0\right\}$ GO TO 2
10. If the step was rejected, compute a smaller substep:
    $\Delta T \leftarrow \Delta T^{(k)} = \Delta T^{(k)} \cdot max\left\{0.9\left[\dfrac{TOL}{R^{(k)}}\right]^{1/2}, 0.1\right\}$ GO TO 2
11. Return the final stress and hardening states:
    $\sigma = \hat{\sigma}^{(k)}, \quad \kappa^{(k)} = \hat{\kappa}^{(k)}$

0	0					
$\frac{1}{5}$	$\frac{1}{5}$					
$\frac{3}{10}$	$\frac{3}{40}$	$\frac{9}{40}$				
$\frac{4}{5}$	$\frac{44}{45}$	$-\frac{56}{15}$	$\frac{32}{9}$			
$\frac{8}{9}$	$\frac{19372}{6561}$	$-\frac{25360}{2187}$	$\frac{64448}{6561}$	$-\frac{212}{729}$		
1	$\frac{9017}{3168}$	$-\frac{355}{33}$	$\frac{46732}{5247}$	$\frac{49}{176}$	$-\frac{5103}{18656}$	
σ	$\frac{35}{384}$	0	$\frac{500}{113}$	$\frac{125}{192}$	$-\frac{2187}{6784}$	$\frac{11}{84}$
$\hat{\sigma}$	$\frac{5779}{57600}$	0	$\frac{7571}{16695}$	$\frac{393}{640}$	$-\frac{92097}{339200}$	$\frac{187}{2100}$

Fig. 3. Coefficients for Runge–Kutta–Dormand–Prince scheme.

work of Wallin and Ristinmaa [22]. The whole integration process is similar to the modified Euler scheme except that the fourth and fifth order Runge–Kutta–Dormand–Prince algorithms are used to estimate the new stresses and hardening parameter like:

$$\sigma = \sigma_0 + \tfrac{35}{384}\Delta\sigma_1 + \tfrac{500}{1113}\Delta\sigma_3 + \tfrac{125}{192}\Delta\sigma_4 - \tfrac{2187}{6784}\Delta\sigma_5 + \tfrac{11}{84}\Delta\sigma_6,$$
$$\kappa = \kappa_0 + \tfrac{35}{384}\Delta\kappa_1 + \tfrac{500}{1113}\Delta\kappa_3 + \tfrac{125}{192}\Delta\kappa_4 - \tfrac{2187}{6784}\Delta\kappa_5 + \tfrac{11}{84}\Delta\kappa_6,$$
$$\hat{\sigma} = \sigma_0 + \tfrac{5779}{57\,600}\Delta\sigma_1 + \tfrac{7571}{16\,695}\Delta\sigma_3 + \tfrac{393}{640}\Delta\sigma_4 - \tfrac{92097}{339\,200}\Delta\sigma_5 + \tfrac{187}{2100}\Delta\sigma_6,$$
$$\hat{\kappa} = \kappa_0 + \tfrac{5779}{57\,600}\Delta\kappa_1 + \tfrac{7571}{16\,695}\Delta\kappa_3 + \tfrac{393}{640}\Delta\kappa_4 - \tfrac{92097}{339\,200}\Delta\kappa_5 + \tfrac{187}{2100}\Delta\kappa_6,$$

in which

$$\Delta\sigma_i = D_{ep}(\sigma_{i-1}, \kappa_{i-1})\Delta\varepsilon,$$
$$\Delta\kappa_i = \Delta\lambda(\sigma_{i-1}, \kappa_{i-1}, \Delta\varepsilon)h_{i-1}$$

with

$$\sigma_1 = \sigma_0 + \tfrac{1}{5}\Delta\sigma_1,$$
$$\kappa_1 = \kappa_0 + \tfrac{1}{5}\Delta\kappa_1,$$
$$\sigma_2 = \sigma_0 + \tfrac{3}{40}\Delta\sigma_1 + \tfrac{9}{40}\Delta\sigma_2,$$
$$\kappa_2 = \kappa_0 + \tfrac{3}{40}\Delta\kappa_1 + \tfrac{9}{40}\Delta\kappa_2,$$
$$\sigma_3 = \sigma_0 + \tfrac{44}{45}\Delta\sigma_1 - \tfrac{56}{15}\Delta\sigma_2 + \tfrac{32}{9}\Delta\sigma_3,$$
$$\kappa_3 = \kappa_0 + \tfrac{44}{45}\Delta\kappa_1 - \tfrac{56}{15}\Delta\kappa_2 + \tfrac{32}{9}\Delta\kappa_3,$$
$$\sigma_4 = \sigma_0 + \tfrac{19\,372}{6561}\Delta\sigma_1 - \tfrac{25\,360}{2187}\Delta\sigma_2 + \tfrac{64\,448}{6561}\Delta\sigma_3 - \tfrac{212}{729}\Delta\sigma_4,$$
$$\kappa_4 = \kappa_0 + \tfrac{19\,372}{6561}\Delta\kappa_1 - \tfrac{25\,360}{2187}\Delta\kappa_2 + \tfrac{64\,448}{6561}\Delta\kappa_3 - \tfrac{212}{729}\Delta\kappa_4,$$
$$\sigma_5 = \sigma_0 + \tfrac{9017}{3168}\Delta\sigma_1 - \tfrac{355}{33}\Delta\sigma_2 - \tfrac{46\,732}{5247}\Delta\sigma_3 + \tfrac{49}{176}\Delta\sigma_4 - \tfrac{5103}{18\,656}\Delta\sigma_5,$$
$$\kappa_5 = \kappa_0 + \tfrac{9017}{270}\Delta\kappa_1 - \tfrac{355}{33}\Delta\kappa_2 - \tfrac{46\,732}{5247}\Delta\kappa_3 + \tfrac{49}{176}\Delta\kappa_4 - \tfrac{5103}{18\,656}\Delta\kappa_5,$$

The Runge–Kutta–Dormand–Prince algorithm, which incorporates error control and a variable step size for each integration point, may be summarized as in Table 4.

The detailed introduction of these two integration schemes can be found in Ref. [9,12]. For a single substep, the modified Euler scheme and Runge–Kutta–Dormand–Prince scheme require two and six evaluations of D_{ep}, respectively. Since its high order, the Runge–Kutta–Dormand–Prince scheme will be chosen for implementing the ''ideal'' run.

4. Numerical experiment

In order to illustrate the performance of the proposed algorithms in the finite element analysis, a subroutine for ABAQUS/Explicit [23] was developed and have been applied to a typical three-dimensional deep-cup drawing process, which is one of the benchmark problems in sheet metal forming industry. Fig. 4 shows a flow chart of stress integration process in user subroutine (VUMAT).

Fig. 5 shows a schematic description of the tools. The blank is initially square, 200 mm by 200 mm. The die is a flat surface with a square hole 102.5 mm by 102.5 mm, rounded at the edges with a radius of 10 mm. The square punch measures 100 mm by 100 mm and is rounded at the edges with the same 10 mm radius. A load of 20 000 N is applied to the blank holder. The blank holder is then

Table 4
Runge–Kutta–Dormand–Prince scheme with subincrements

1. Determine the initial state for σ, κ, substep counter k, time T and its increment ΔT:
   $\sigma = \sigma_0, \quad \kappa = \kappa_0, \quad k = 10, \quad T = 0, \quad \Delta T = 1$
2. While $T \leqslant 1$, perform 3 to 10. Otherwise go to 11.
3. Determine the substep size:
   $\Delta\varepsilon^{(k)} = \Delta T \Delta\varepsilon$
4. Calculate $\Delta\sigma_i$ and $\Delta\kappa_i$ for i from 1 to 6 according to:
   $\delta\sigma_i = D_{ep}(\sigma_i, \kappa_i)\Delta\varepsilon^{(k)}$

   $\delta\kappa_i = \Delta\lambda(\sigma_i, \kappa_i)h$
5. Compute approximate solutions for $\sigma^{(k)}$ and $\kappa^{(k)}$:
   $\sigma^{(k)} = \sigma^{(k-1)} + \frac{31}{540}\Delta\sigma_1 + \frac{190}{297}\Delta\sigma_3 - \frac{145}{108}\Delta\sigma_4 + \frac{351}{220}\Delta\sigma_5 + \frac{1}{20}\Delta\sigma_6$

   $\kappa^{(k)} = \sigma^{(k-1)} + \frac{31}{540}\Delta\kappa_1 + \frac{190}{297}\Delta\kappa_3 - \frac{145}{108}\Delta\kappa_4 + \frac{351}{220}\Delta\kappa_5 + \frac{1}{20}\Delta\kappa_6$

   $\hat{\sigma}^{(k)} = \sigma^{(k-1)} + \frac{19}{216}\Delta\sigma_1 + \frac{1000}{2079}\Delta\sigma_3 - \frac{125}{216}\Delta\sigma_4 + \frac{81}{88}\Delta\sigma_5 + \frac{5}{56}\Delta\sigma_6$

   $\hat{\kappa}^{(k)} = \sigma^{(k-1)} + \frac{19}{216}\Delta\kappa_1 + \frac{1000}{2079}\Delta\kappa_3 - \frac{125}{216}\Delta\kappa_4 + \frac{81}{88}\Delta\kappa_5 + \frac{5}{56}\Delta\kappa_6$
6. Compute the estimate of the relative error for the current substep:
   $R^{(k)} = \|\hat{\sigma}^{(k)} - \sigma^{(k)}\| / \|\hat{\sigma}^{(k)}\|$
7. Check if the current substep is accepted or rejected:
   IF $R^{(k)} > TOL$ GO TO 10
8. Update the stress, hardening parameter and integration time:
   $\sigma^{(k)} = \hat{\sigma}, \quad \kappa^{(k)} = \hat{\kappa}, \quad T = T + \Delta T$
9. Evaluate next substep size:
   $\Delta T \leftarrow \Delta T^{(k+1)} = \Delta T^{(k)} \cdot min\{0.9[TOL/R^{(k)}]^{1/5}, 2.0\}$ GO TO 2
10. If the step was rejected, compute a smaller substep:
    $\Delta T \leftarrow \Delta T^{(k)} = \Delta T^{(k)} \cdot max\{0.9[TOL/R^{(k)}]^{1/5}, 0.1\}$ GO TO 2
11. Return the final stress and hardening states:
    $\sigma = \hat{\sigma}^{(k)}, \quad \kappa^{(k)} = \hat{\kappa}^{(k)}$

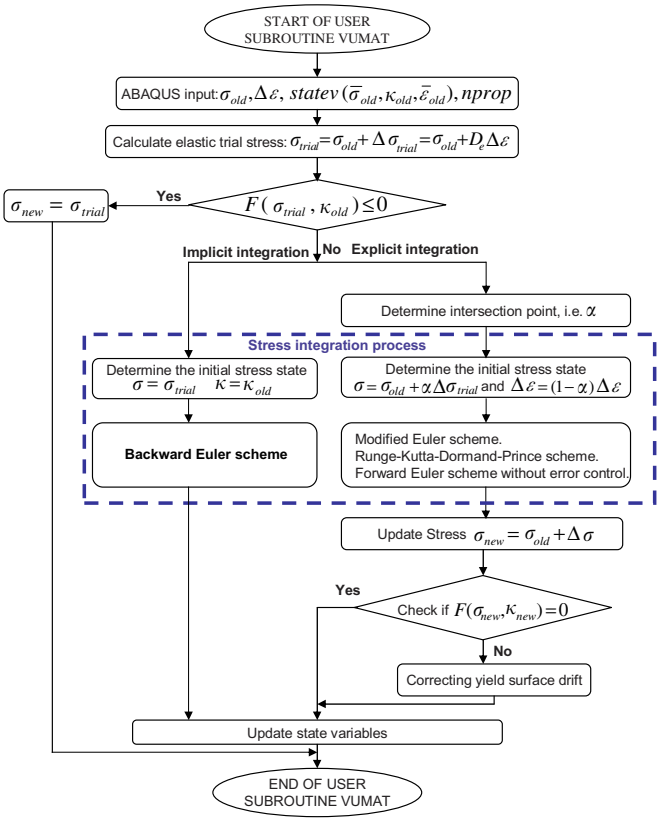

Fig. 4. Schematic flow chart of the stress integration process.

Fig. 5. Schematic illustration of the tools and blank for the deep-cup drawing process.

allowed to move only in the vertical direction to accommodate changes in the blank thickness. The drawing process is simulated by moving the punch downward through a total distance of 36 mm in 0.0036 s. Owing to the symmetry of the material, only one-quarter of the structure is modelled. The FE mesh of the blank is composed of 1225 elements (4-node, reduced integration, doubly curved shell elements with five integration points through the shell section, called S4R in ABAQUS nomenclature [23]). The tools are meshed with 4-node, bilinear quadrilateral, rigid elements, called R3D4 in ABAQUS.

An associated flow rule is assumed. The Swift hardening law between effective stress $\bar{\sigma}$ and effective plastic strain $\bar{\varepsilon}_p$ is employed, i.e.

$$\bar{\sigma} = K(\varepsilon_0 + \bar{\varepsilon}_p)^n, \tag{45}$$

where n is the strain-hardening exponent and K and ε_0 are material constants. The material properties are taken as follows: mild steel, thickness 0.82 mm, Young's modulus

$E = 206\,\text{GPa}$, Poisson's ratio $v = 0.33$, uniaxial true stress–true strain curve $\bar{\sigma} = 567.29(0.007127 + \bar{\varepsilon}_p)^{0.2637}$ MPa, friction coefficient $\mu = 0.16$.

In order to test the influence of different tolerance on the accuracy, an "ideal" run is implemented with the same mesh, the same material properties and the same global solution technique, but the Runge–Kutta–Dormand–Prince substepping scheme is used to integrate the constitutive law. The tolerance is set to be very small (10^{-10}). Even though the number of the substeps is sufficient high and the drift from the yield surface can be ignored, the stress correction are still used to ensure the accuracy of the "ideal" run. These "ideal" result is used to compare with the implicit return scheme, Runge–Kutta–Dormand–Prince method and modified Euler scheme with different tolerances. The errors in the elastic–plastic stresses are computed using

$$Error = \frac{\left[\sum_{i=1}^{N}(\sigma_i - \sigma_i^{ideal})^2\right]^{1/2}}{\left[\sum_{i=1}^{N}(\sigma_i^{ideal})^2\right]^{1/2}},$$

where N is the total number of the integration points. For each explicit scheme, two different models are studied, i.e. with and without stress correction, respectively.

Note that in all the following figures and tables, BE, FE, ME and RKDP denote the backforward Euler scheme, forward Euler scheme, modified Euler scheme and Runge–Kutta–Dormand–Prince scheme, respectively. FEC, MEC and RKDPC mean that stress correction is applied for these schemes.

4.1. Von Mises yield criteria

Our first constitutive model used to test the integration schemes is Von Mises yield surface and the yield function is set:

$$F(\sigma, \bar{\varepsilon}_p) = \sqrt{3}(J_2')^{1/2} - \bar{\sigma} \tag{46}$$

with

$$\begin{aligned} J_2 &= \tfrac{1}{2}S : S \\ &= \tfrac{1}{6}[(\sigma_1 - \sigma_2)^2 + (\sigma_2 - \sigma_3)^2 + (\sigma_3 - \sigma_1)^2] \\ &= \tfrac{1}{2}[\sigma_{xx}'^2 + \sigma_{yy}'^2 + \sigma_{zz}'^2] + \sigma_{xy}^2 + \sigma_{yz}^2 + \sigma_{xz}^2, \end{aligned} \tag{47}$$

in which S is the deviatoric stress:

$$S = \sigma_{ij}' = \sigma_{ij} - \tfrac{1}{3}\delta_{ij}\sigma_{kk}. \tag{48}$$

4.1.1. Accuracy

The differences of the results obtained from proposed integration schemes can be seen clearly from the effective stress and thickness contours of some models in Figs. 6–17 In Figs. 18 and 19, we present strain–stress curve for the deep-cup drawing process. The thickness strains are plotted in Figs. 20 and 21. With reference to these figures, we can find that, for the cases of large plastic strain problem, the

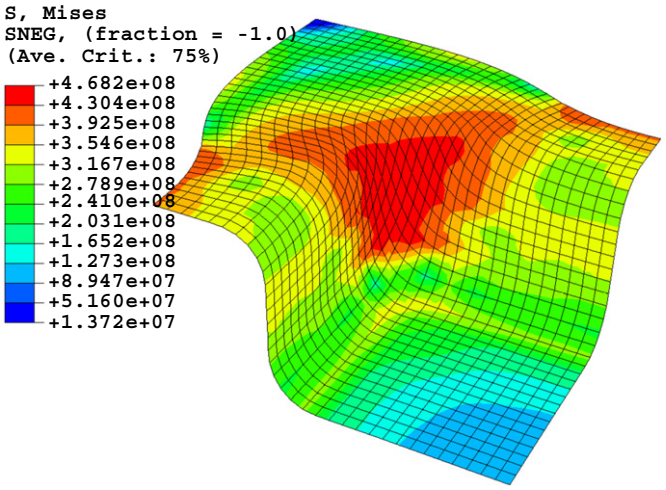

Fig. 6. Contour of the effective stress from "ideal run" (Von Mises model).

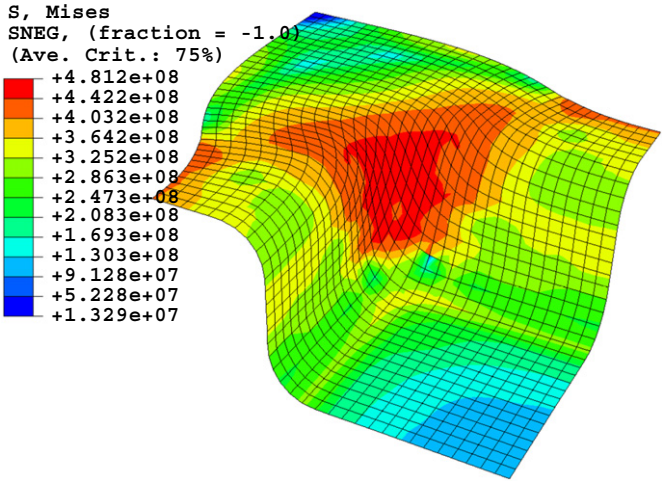

Fig. 7. Contour of the effective stress from FE with stress correction (Von Mises model).

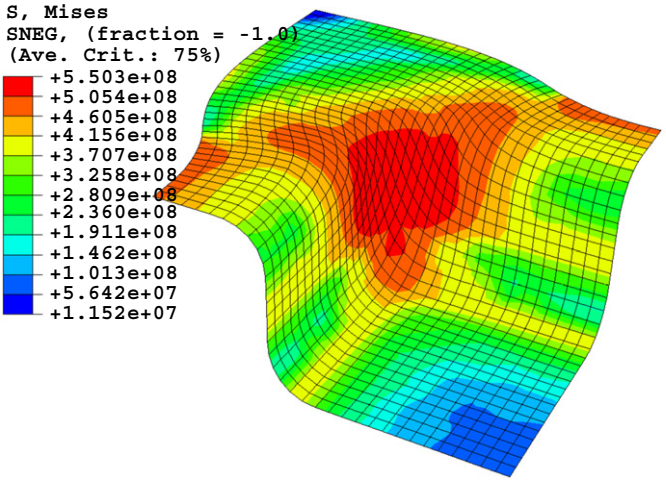

Fig. 8. Contour of the effective stress from ME (10^{-4}) without stress correction (Von Mises model).

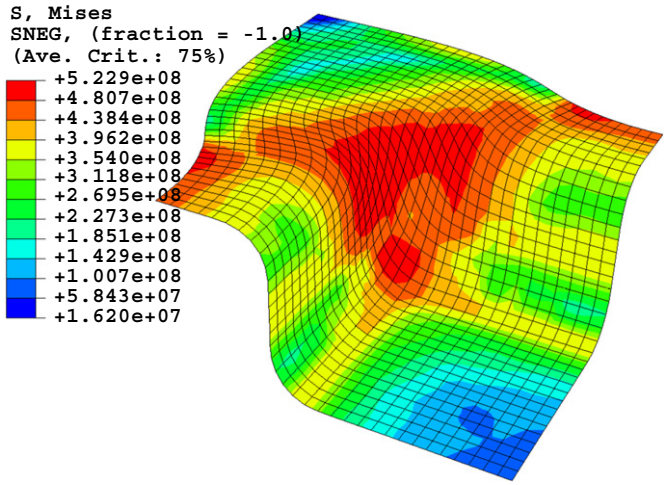

Fig. 9. Contour of the effective stress from RKDP (10^{-4}) without stress correction (Von Mises model).

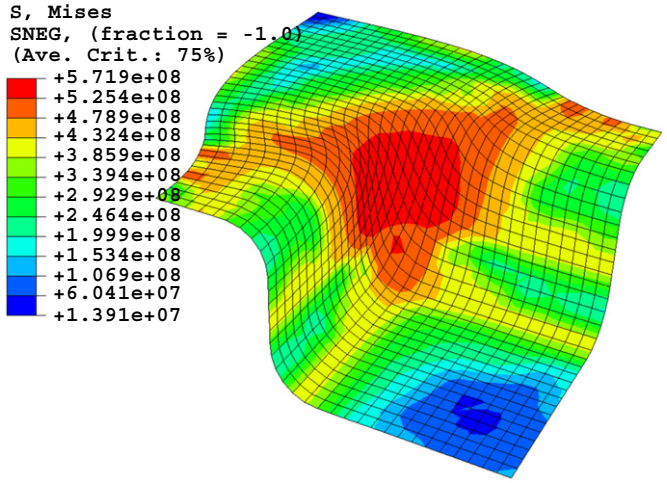

Fig. 10. Contour of the effective stress from ME (10^{-2}) without stress correction (Von Mises model).

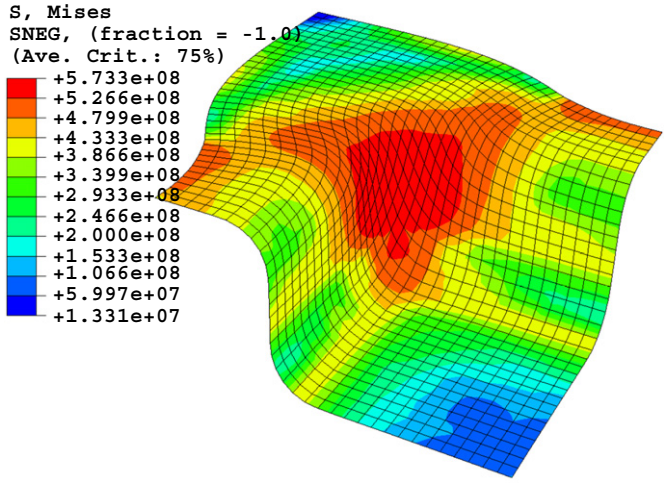

Fig. 11. Contour of the effective stress from FE without stress correction (Von Mises model).

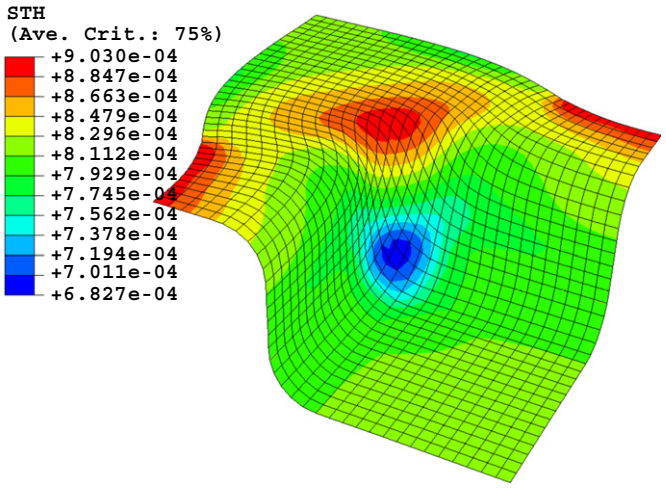

Fig. 12. Contour of the blank thickness from "ideal" run (Von Mises model).

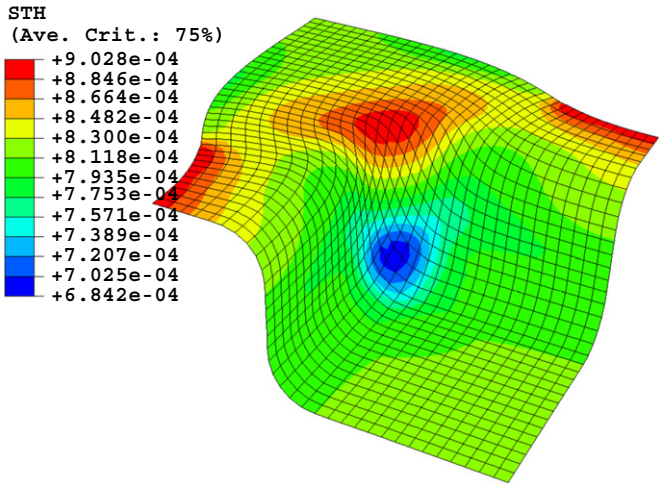

Fig. 13. Contour of the blank thickness from FE with stress correction (Von Mises model).

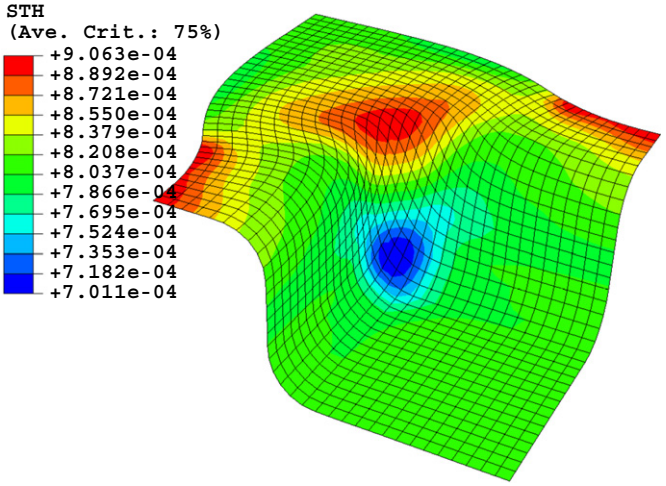

Fig. 14. Contour of the blank thickness from ME (10^{-4}) without stress correction (Von Mises model).

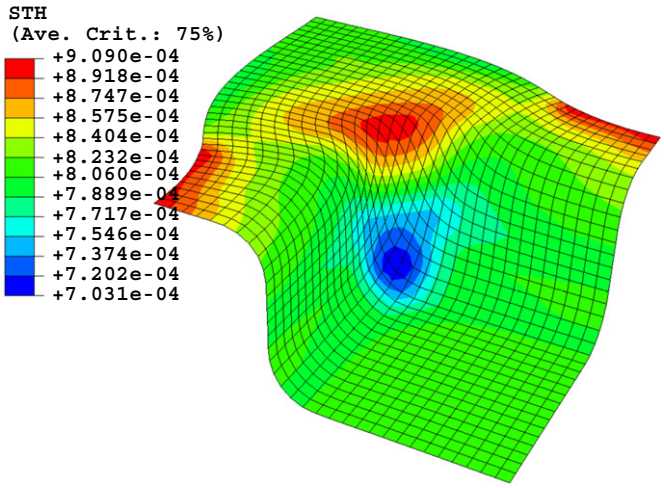

Fig. 15. Contour of the blank thickness from RKDP (10^{-4}) without stress correction (Von Mises model).

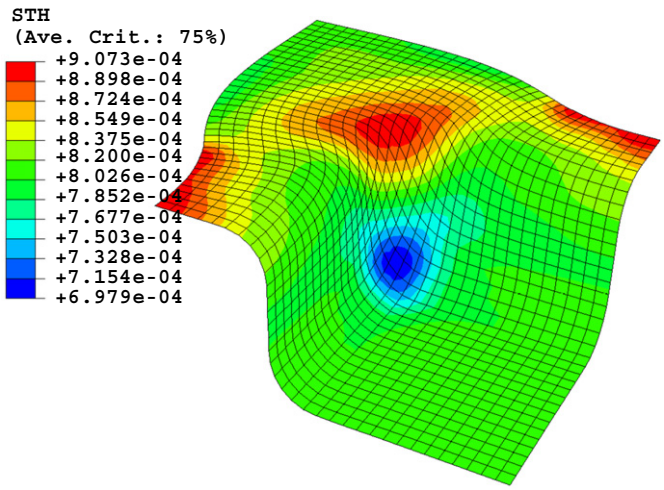

Fig. 16. Contour of the blank thickness from ME (10^{-2}) without stress correction (Von Mises model).

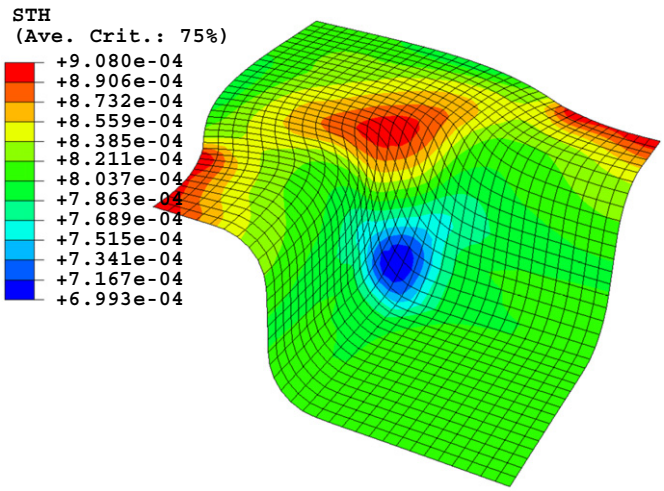

Fig. 17. Contour of the blank thickness from FE without stress correction (Von Mises model).

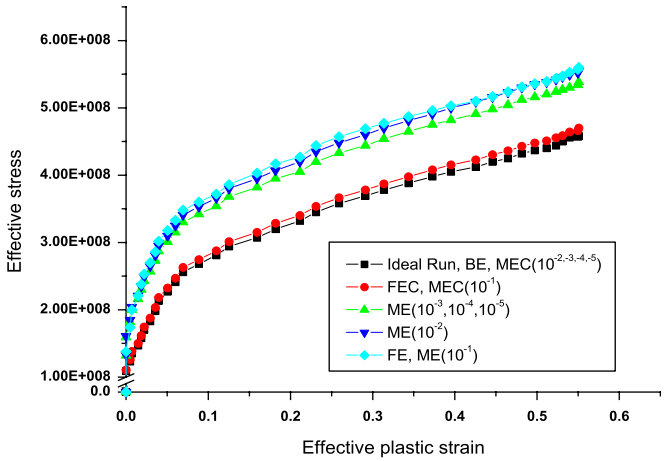

Fig. 18. Effective plastic strain–effective stress curves for BE, FE, FEC, ME, MEC (Von Mises model).

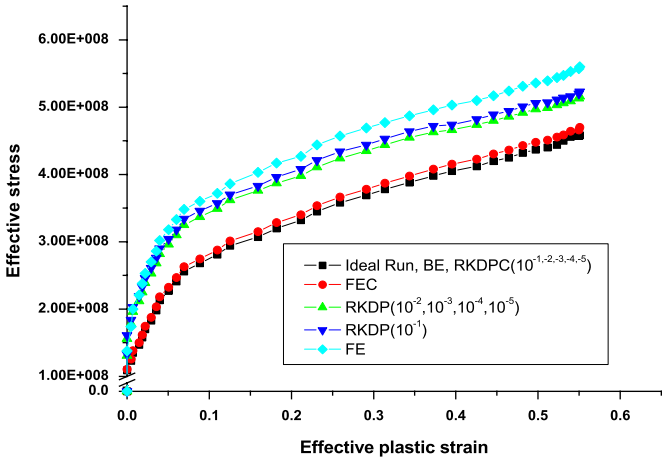

Fig. 19. Effective plastic strain–effective stress curves for BE, FE, FEC, RKDP, RKDPC (Von Mises model).

results computed by the explicit schemes without stress correction are almost same no matter how tight we set the error tolerance. However, the results are completely different if the stress correction is employed. In fact, without stress correction, all the three explicit schemes cannot give the satisfactory accuracy for the case which involves strain hardening when the tolerance is set to be 10^{-5} or larger. We also can see that the forward Euler scheme gives the worst result without the stress correction, and the backward Euler scheme gives relatively accurate result. It is worth noting that even the Runge–Kutta–Dormand–Prince is nearly insensitive to the error tolerance when no stress correction is applied for the deep drawing process, although the accuracy is improved as the error tolerance gets tighter. This again proves that, because the approximation nature of the finite element method, yield surface drift may occur with the stresses moving away from the yield surface. This deviation is practically independent of the integration scheme adopted. When the model involves strain (work) hardening where the yield surface

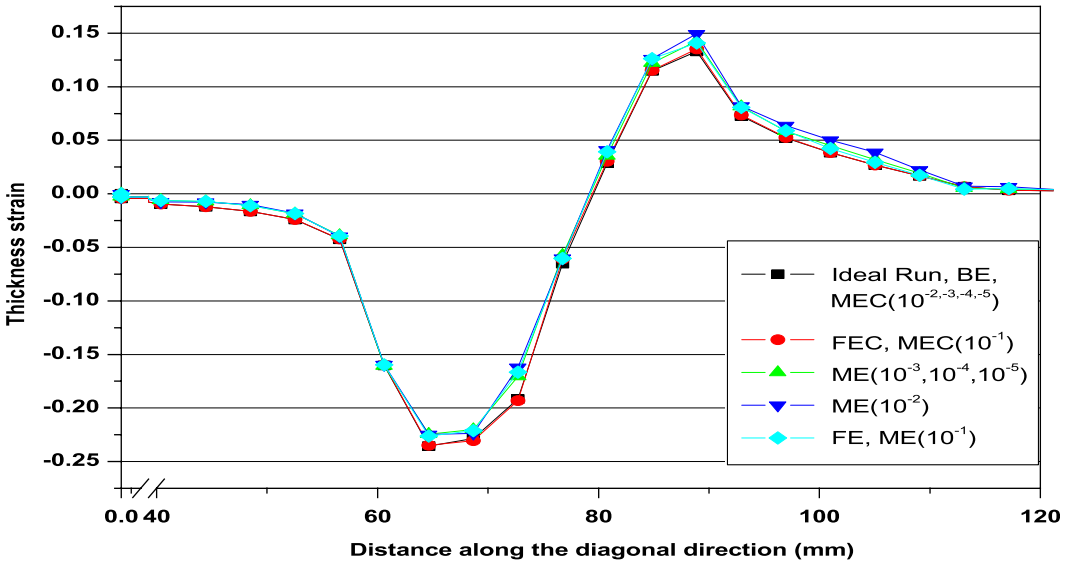

Fig. 20. Plot of thickness strain for BE, FE, FEC, ME, MEC (Von Mises model).

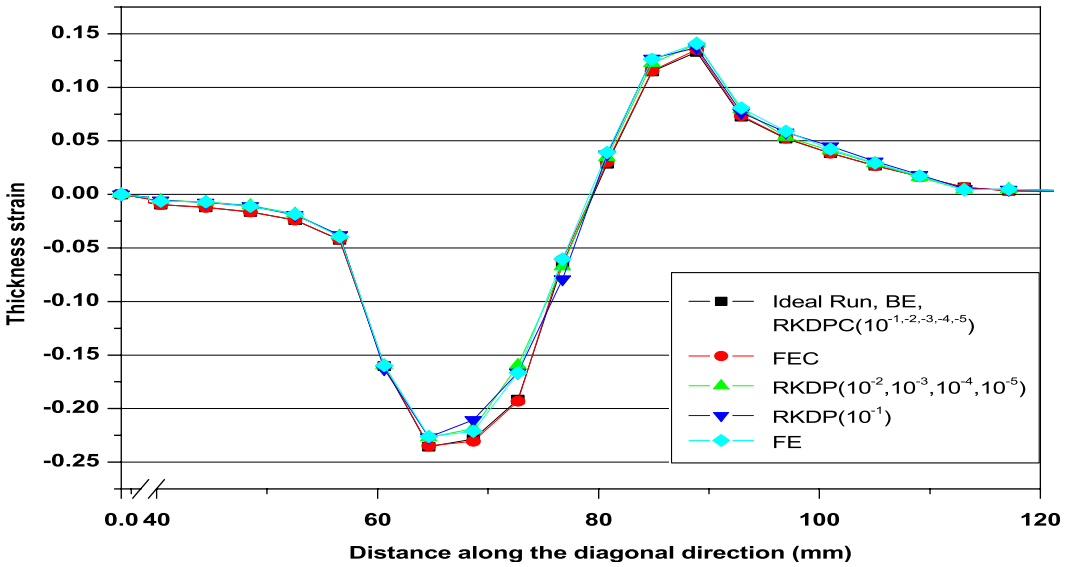

Fig. 21. Plot of thickness strain for BE, FE, FEC, RKDP, RKDPC (Von Mises model).

is moving with loading increment, the drift is more significant. Since such discrepancies are usually cumulative, it is important to ensure that the stresses are corrected back to the current yield surface at each step of the integration. Since we apply the stress correction at the end of each time increment, it does not improve the accuracy significantly when the error caused by the integration scheme is too serious. This is demonstrated by the forward Euler scheme and the modified Euler scheme with tolerance of 10^{-1}. However, it can make the computed stress to fulfill the consistency condition at the end of load increment and avoid error accumulation and therefore instabilities in the following time increments.

The errors in the computed stresses from different algorithms with different tolerance are listed in Table 5. With reference to Table 5, it can be seen that, the backward Euler scheme gives good result which is adequate for the engineering computation, compared with the explicit schemes. All the explicit schemes give incorrect results if no stress correction is applied, although the accuracy can be improved slightly as the tolerance decreases for both the modified Euler scheme and the Runge–Kutta–Dormand–Prince scheme. For the cases in which stress correction is applied for the explicit schemes, all the explicit schemes give the better results than the return algorithm does if the integration error can be controlled to some extent, i.e. for the modified Euler scheme with tolerance of 10^{-5} and the Runge–Kutta–Dormand–Prince scheme with the tolerance of 10^{-3} or smaller. In Ref. [8], the measure of error which is approximately equal to tolerance was achieved. However,

Table 5
Results of errors for BE, FE, ME and RKDP with different tolerance (Von Mises model)

Method					Error
BE					1.34×10^{-2}
FE					8.26×10^{-1}
FEC					6.72×10^{-2}
	Error tolerance				
	10^{-1}	10^{-2}	10^{-3}	10^{-4}	10^{-5}
ME	9.54×10^{-1}	8.23×10^{-1}	5.84×10^{-1}	5.36×10^{-1}	5.37×10^{-1}
MEC	5.12×10^{-2}	2.56×10^{-2}	2.54×10^{-2}	1.58×10^{-2}	8.42×10^{-3}
RKDP	3.12×10^{-1}	2.09×10^{-1}	1.76×10^{-1}	1.78×10^{-1}	1.54×10^{-1}
RKDPC	2.38×10^{-2}	2.39×10^{-2}	6.13×10^{-3}	6.87×10^{-3}	6.35×10^{-3}

Table 6
Total substeps needed in the overall solution for ME and RKDP schemes with different tolerance (Von Mises model)

	Error tolerance				
	10^{-1}	10^{-2}	10^{-3}	10^{-4}	10^{-5}
ME	46 954 562	46 934 813	46 946 482	55 674 653	87 665 434
MEC	46 836 448	46 875 346	46 925 948	52 783 446	81 970 435
RKDP	46 816 128	46 785 441	46 786 154	46 788 647	47 343 496
RKDPC	46 807 413	46 768 141	46 747 980	46 747 643	47 302 996

Table 7
CPU time (s) spent on the overall solution (Von Mises model)

Method					CPU time (s)
BE					336
FE					396
FEC					392
	Error tolerance				
	10^{-1}	10^{-2}	10^{-3}	10^{-4}	10^{-5}
ME	376	375	375	432	558
MEC	374	374	373	418	469
RKDP	596	597	614	636	657
RKDPC	513	508	514	514	526

as mentioned previously, the results obtained from modified Euler scheme and Runge–Kutta–Dormand–Prince scheme are not improved as the error tolerance becomes tighter. This again indicates that the stress correction applied at the end of each load increment does not improve the performance significantly unless the integration error is controlled to some extent.

4.1.2. Efficiency

In Table 6, we list the total number of substeps for overall solution of the modified Euler scheme and Runge–Kutta–Dormand–Prince scheme. The corresponding CPU time spent on overall solution is listed in Table 7. We can see that, the Runge–Kutta–Dormand–Prince scheme generally requires less substeps than the modified Euler scheme for the fixed value of tolerance. For the tolerance which is from 10^{-3} to 10^{-4}, the Runge–Kutta–Dormand–Prince scheme uses approximately half the number of substeps consumed by the modified Euler scheme. This confirms that the high-order Runge–Kutta–Dormand–Prince scheme does not need more substeps to obtain the prescribed accuracy. However, since the Runge–Kutta–Dormand–Prince scheme usually needs to compute elastic–plastic matrix six times for each substep, it still consumes more CPU time than the modified Euler scheme does. It is interesting to see that the use of stress correction not only improves the accuracy, but saves the computational time significantly. It can be seen in Table 7 that for both modified Euler scheme and Runge–Kutta–Dormand–Prince scheme, the CPU time is greatly reduced when the stress correction is used. This is probably because the stress states are integrated more accurately when the yield drift is corrected back to yield surface at the end of each load increment, causing no more effort spent on trying to correct the accumulative errors in the following increments. Note that, unlike in Ref. [8], the Runge–Kutta–England scheme has a significant advantage over the modified Euler scheme, in the present study, the performance of the Runge–Kutta–Dormand–Prince scheme is only slightly better than that of the modified Euler scheme. When the stress correction is employed, the Runge–Kutta–Dormand–Prince scheme is better than the modified Euler scheme in terms of its ability to integrate more accurately with tight tolerance. In spite of this, both schemes can give satisfactory results for the engineering problem if the stress correction is used.

4.2. Hill's yield criteria

Cold-rolled sheet metal often exhibits anisotropic properties in the forming process, which are mostly caused

by preferred orientations of grains developed during the severe plastic deformation such as cold rolling. The quadratic yield function of Hill [24] is still a commonly employed phenomenological approach to predict anisotropy in sheet metal forming operations despite its incapability to predict the so-called experimentally observed anomalous behavior.

Hill's stress potential is a simple extension of the Mises function to allow anisotropic behavior. This function is

$$F(\sigma) = \sqrt{\begin{array}{c} F(\sigma_y-\sigma_z)^2 + G(\sigma_z-\sigma_x)^2 + H(\sigma_x-\sigma_y)^2 + 2L\sigma_{yz}^2 \\ +2M\sigma_{zx}^2 + 2N\sigma_{xy}^2, \end{array}}$$

where F, G, H, L, M and N are material constants obtained by tests of the material in different directions. These constants are given as follows:

$$F = 0.283, \quad G = 0.358, \quad H = 0.642,$$
$$L = M = N = 1.288.$$

4.2.1. Accuracy

For demonstration, we present the effective stress and thickness contours for some of the models with relatively large differences of the results in Figs. 22–33. The differences of the results obtained from different integration schemes using Hill's yield criterion can be seen clearly in these figures. Again, we present effective plastic strain—effective stress curves in Figs. 34 and 35 and the thickness strains are shown in Figs. 36 and 37. The results once more demonstrate that for Hill's model, all the explicit schemes give inaccurate results when no stress correction is applied, no matter how tight the tolerance is. However, for such complex constitutive model, some of the models, i.e. ME with tolerance of 10^{-1} and 10^{-2} and RKDP with tolerance of 10^{-1}, still produce unsatisfactory results even with the help of the stress correction.

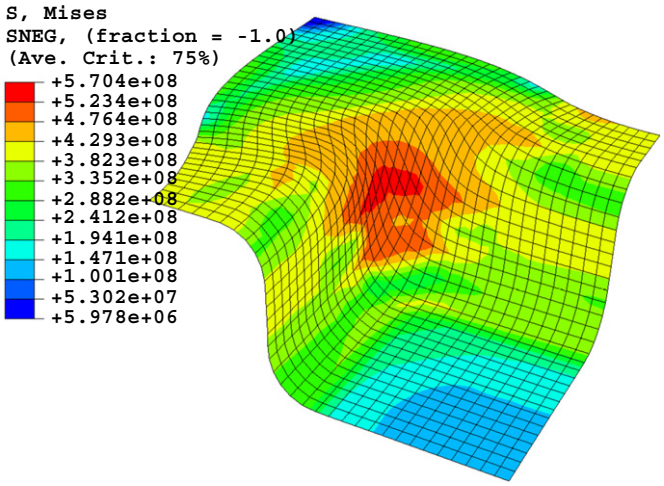

Fig. 22. Contour of the effective stress from "ideal run" (Hill's model).

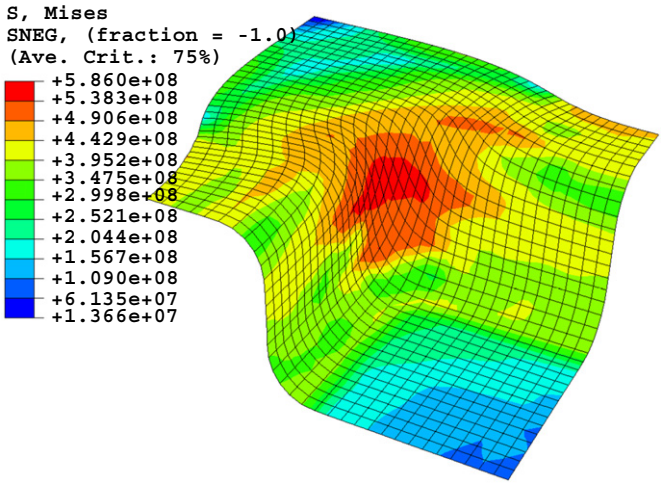

Fig. 23. Contour of the effective stress from FE with stress correction (Hill's model).

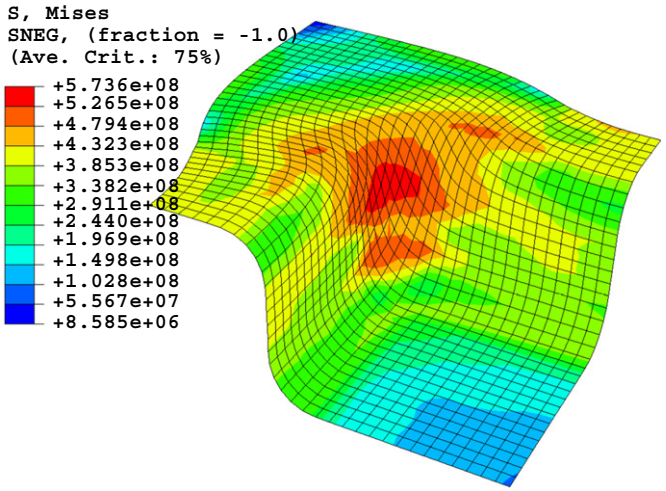

Fig. 24. Contour of the effective stress from ME (10^{-4}) with stress correction (Hill's model).

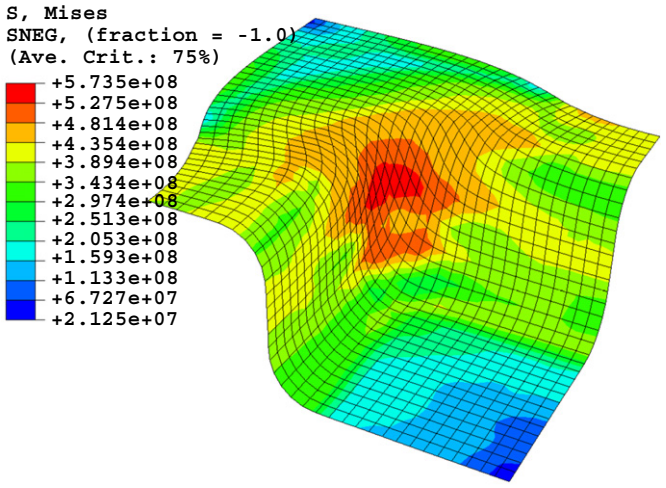

Fig. 25. Contour of the effective stress from RKDP (10^{-2}) with stress correction (Hill's model).

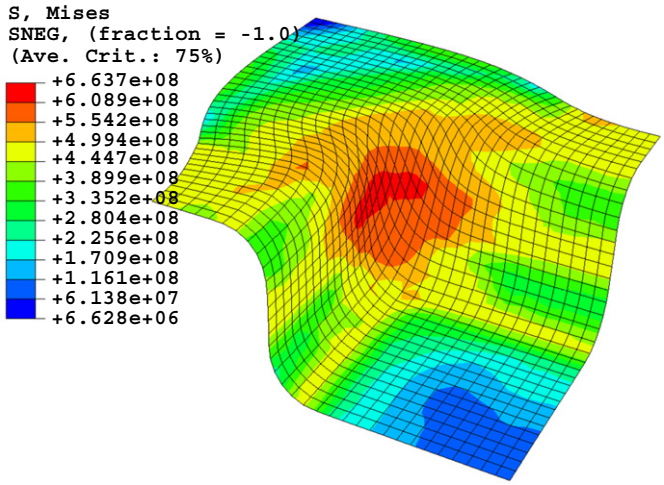

Fig. 26. Contour of the effective stress from ME (10^{-4}) without stress correction (Hill's model).

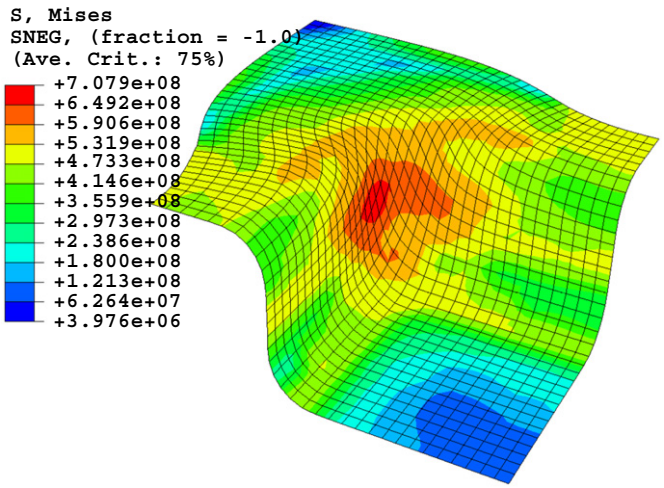

Fig. 27. Contour of the effective stress from FE without stress correction (Hill's model).

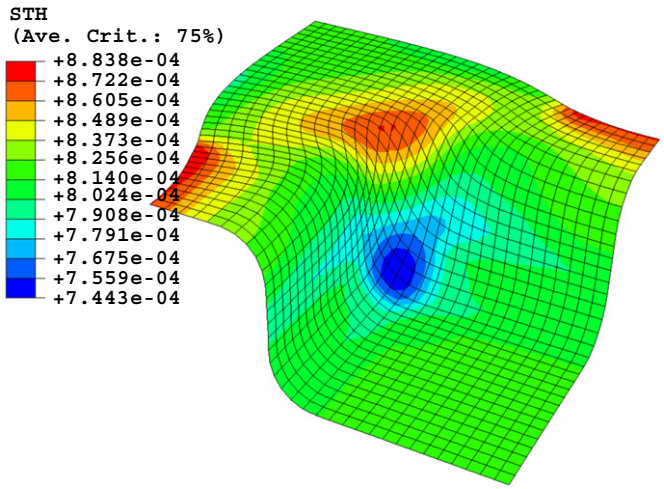

Fig. 28. Contour of the blank thickness from "ideal" run (Hill's model).

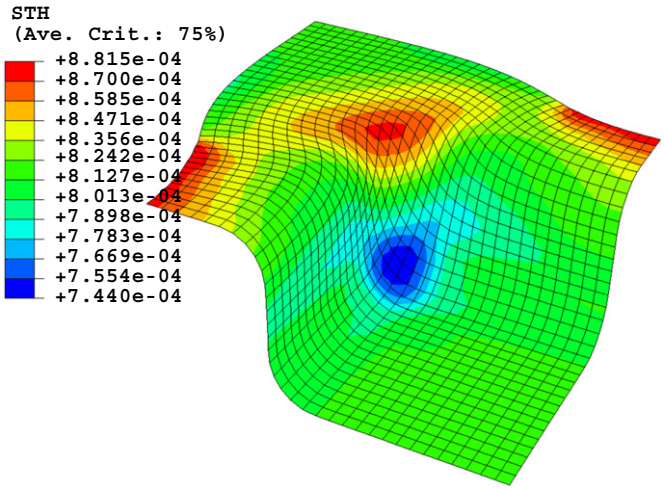

Fig. 29. Contour of the blank thickness from FE with stress correction (Hill's model).

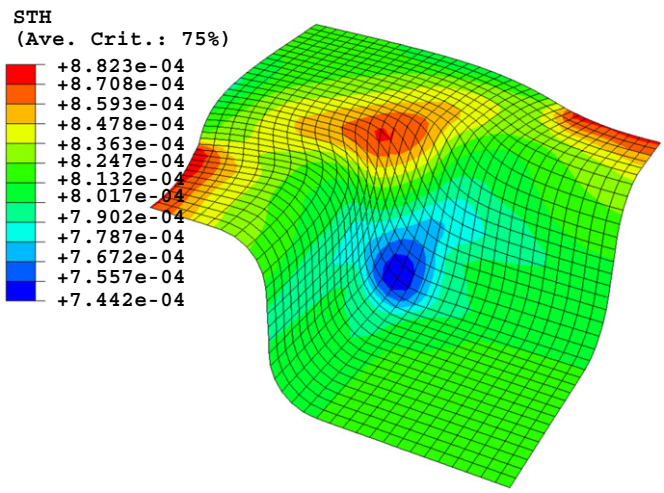

Fig. 30. Contour of the blank thickness from ME (10^{-4}) with stress correction (Hill's model).

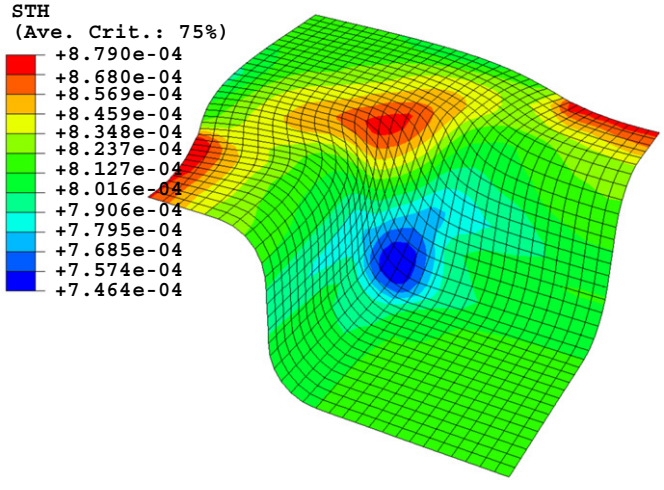

Fig. 31. Contour of the blank thickness from RKDP (10^{-2}) with stress correction (Hill's model).

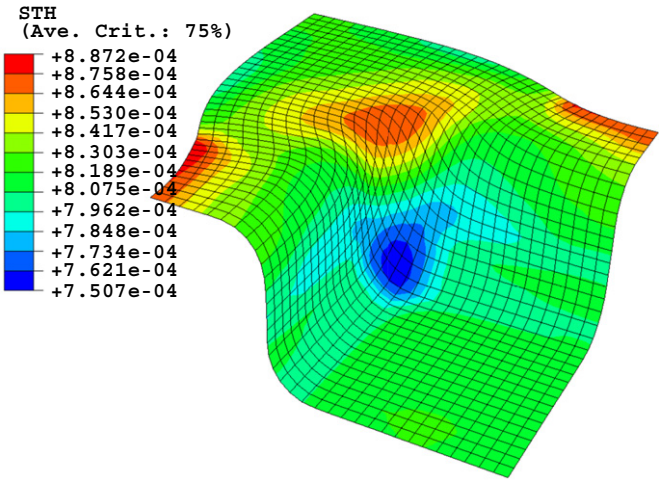

Fig. 32. Contour of the blank thickness from ME (10^{-4}) without stress correction (Hill's model).

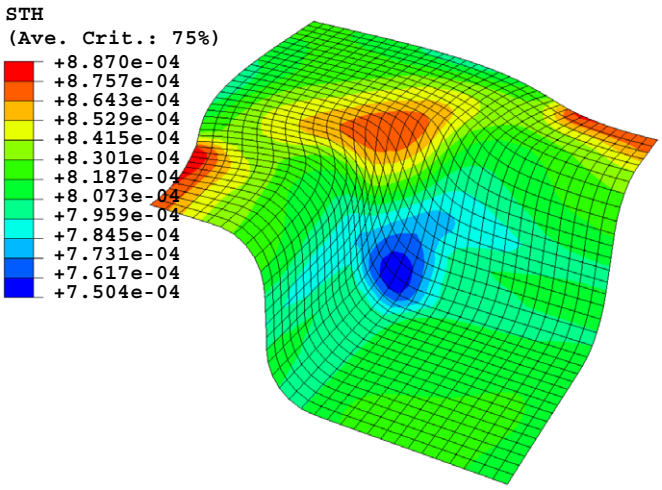

Fig. 33. Contour of the blank thickness from FE without stress correction (Hill's model).

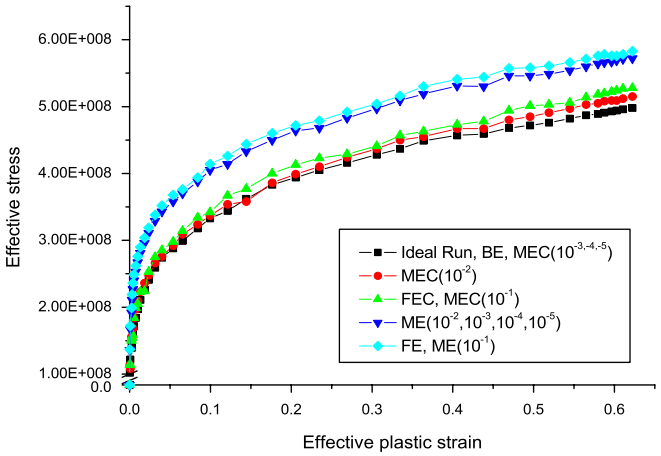

Fig. 34. Effective plastic strain–effective stress curves for BE, FE, FEC, ME, MEC (Hill's model).

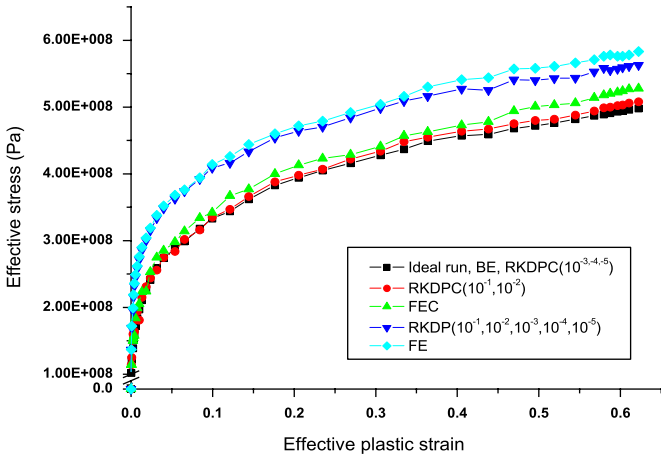

Fig. 35. Effective plastic strain–effective stress curves for BE, FE, FEC, RKDP, RKDPC (Hill's model).

With reference to the errors in the computed stresses from different algorithms shown in Table 8, we can see again that the backward Euler scheme can provide accuracy which is superior to all the explicit schemes in the case that no stress correction is applied. However, when the stress correction is employed, some of the models, such as ME (10^{-4}, 10^{-5}) and RKDP (10^{-4}, 10^{-5}) can produce same or even better level of accuracy than the backward Euler does. Again, we did not obtain the measure of error which is approximately equal to tolerance, even with the high-order RKDP scheme.

4.2.2. *Efficiency*

We present the total number of substeps for overall solution of the modified Euler scheme and Runge–Kutta–Dormand–Prince scheme in Table 9 and the corresponding CPU time spent on overall solution in Table 10. It can be seen that the results we obtained are similar to the ones from Von Mises model, i.e. the Runge–Kutta–Dormand–Prince scheme generally requires less substeps than the modified Euler scheme does for the fixed value of tolerance. However it uses more CPU time than the modified Euler does due to the six evaluations of the elastic–plastic matrix for each substep. Obviously, this is the cost we have to pay when high level of accuracy is required.

5. Conclusion remarks

In this paper, we present two substepping schemes, modified Euler and Runge–Kutta–Dormand–Prince schemes with local error control, enhanced by the stress correction procedure, for analyzing the elastic–plastic problems using both Von Mises yield criteria and Hill's anisotropic yield criteria. Their performances have been compared with the commonly used implicit and explicit integration schemes, including backward Euler algorithm, forward Euler with subincrementation. This comparison is specifically focused on the sheet metal forming process. Both explicit substepping schemes control the error in the

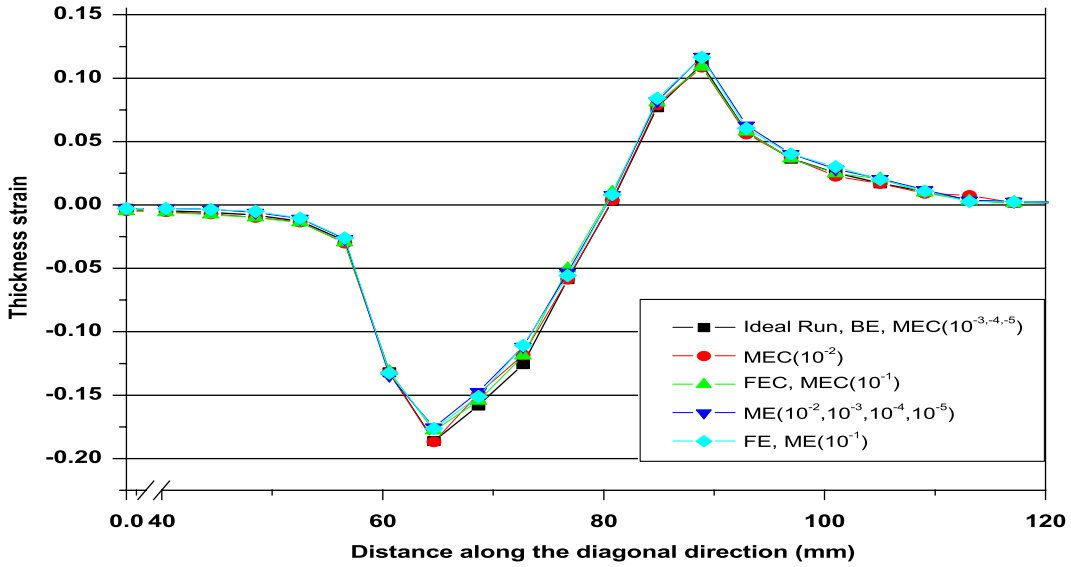

Fig. 36. Plot of thickness strain for BE, FE, FEC, ME, MEC (Hill's model).

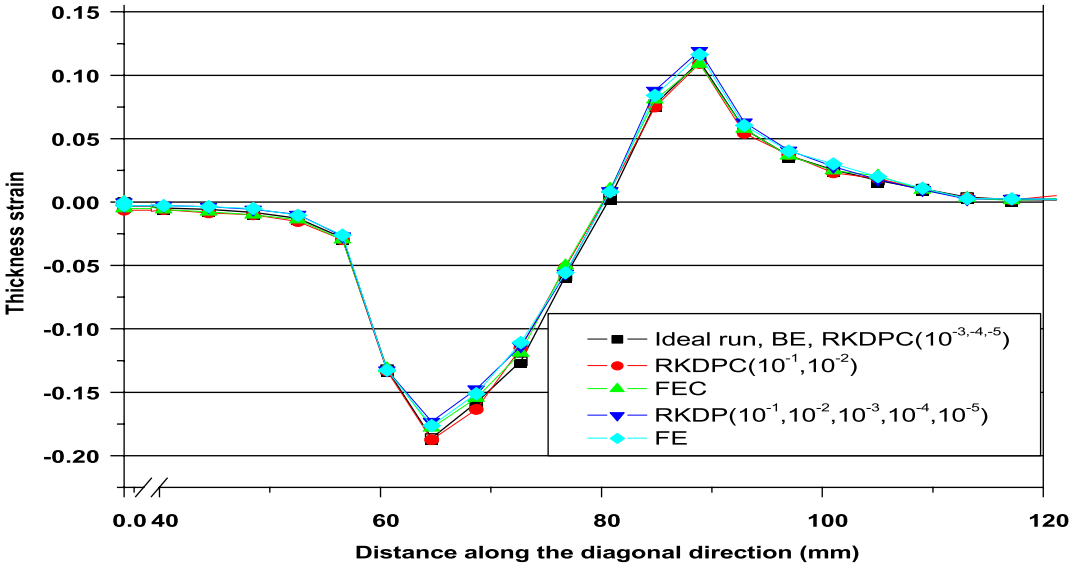

Fig. 37. Plot of thickness strain for BE, FE, FEC, RKDP, RKDPC (Hill's model).

integration process by permitting the size of each substep to vary in accordance with the behavior of the constitutive law. The numerical example indicated that for the three-dimensional sheet metal forming problem of which these two constitutive models are considered, the accuracy can not be improved significantly as the tolerance decreases. Some forms of stress correction should thus be employed in order to ensure that the computed stresses remain on the yield surface at any time and maintain adequate accuracy of the overall solution. It has also been found that applying the stress correction at the end of integration does not increase the computational time significantly, but it can improve the accuracy if the errors during the integration can be reduced to some extent. As more and more complex constitutive model is used for simulating the sheet metal forming process, implementation of the implicit integration on such model could be extremely difficult. In this case, the combination of the substepping scheme with the error control combined with the stress correction method proposed in this paper could offer an alternative way which is efficient and accurate. In summary, the experience suggests that

1. For large strain sheet metal forming problem, neither of the explicit schemes with error control can give accurate result without the application of the stress correction.
2. High-order Runge–Kutta–Dormand–Prince scheme is superior to both the backward Euler scheme and the modified Euler scheme when tight tolerance is employed.

Table 8
Results of errors for BE, FE, ME and RKDP with different tolerance (Hill's model)

Method					Error
BE					3.65×10^{-2}
FE					8.73×10^{-1}
FEC					2.89×10^{-1}
	Error tolerance				
	10^{-1}	10^{-2}	10^{-3}	10^{-4}	10^{-5}
ME	9.03×10^{-1}	6.74×10^{-1}	6.75×10^{-1}	6.74×10^{-1}	6.52×10^{-1}
MEC	2.85×10^{-1}	2.86×10^{-1}	4.12×10^{-2}	3.76×10^{-2}	3.68×10^{-2}
RKDP	5.62×10^{-1}	5.63×10^{-1}	5.62×10^{-1}	5.34×10^{-1}	5.29×10^{-1}
RKDPC	4.56×10^{-1}	4.55×10^{-2}	4.74×10^{-2}	4.06×10^{-2}	8.14×10^{-3}

Table 9
Total substeps needed in the overall solution for ME and RKDP schemes with different tolerance (Hill's Model)

	Error tolerance				
	10^{-1}	10^{-2}	10^{-3}	10^{-4}	10^{-5}
ME	48 256 706	48 258 361	48 264 593	56 247 482	86 196 585
MEC	48 247 453	48 256 488	48 325 473	54 886 242	82 924 864
RKDP	47 689 724	47 445 372	47 446 585	47 447 150	48 245 686
RKDPC	47 671 342	47 438 546	47 435 692	47 432 238	47 119 227

Table 10
CPU time (s) spent on the overall solution (Hill's model)

Method					CPU time (s)
BE					347
FE					395
FEC					382
	Error tolerance				
	10^{-1}	10^{-2}	10^{-3}	10^{-4}	10^{-5}
ME	387	380	389	431	572
MEC	377	368	388	423	476
RKDP	635	639	648	674	692
RKDPC	556	553	563	580	618

3. For the two constitutive models used in this paper, both the modified Euler scheme and the Runge–Kutta–Dormand–Prince scheme in combination with the stress correction can provide same level of accuracy as the backward Euler scheme does. For problems for which high level of accuracy is required, the Runge–Kutta–Dormand–Prince scheme is recommended.
4. To maintain adequate accuracy, tolerance of 10^{-4} or smaller is recommended for the modified Euler scheme. For the Runge–Kutta–Dormand–Prince scheme, the tolerance of 10^{-3} and under is necessary.

Acknowledgments

The authors are grateful to Dr. Zbigniew Stachurski for his helpful discussion and remarks. This work was supported by the Department of Engineering through a scholarship program.

References

[1] Wilkins JL. Calculation of Elastic–plastic Flow. In: Methods of Computational Physics, vol. 8. New York: Academic Press; 1964. p. 211–63.
[2] Krieg RD, Krieg DB. Accuracies of numerical solution methods for the elastic-perfectly plastic-model. Journal of Pressure Vessel Technology 1977;99:510–5.
[3] Ortiz M, Simo JC. An analysis of a new class of integration algorithms for elastoplastic constitutive relations. International Journal for Numerical Methods in Engineering 1986;23:353–66.
[4] Potts DM, Gens A. A critical assessment of methods of correcting for drift from the yield surface in elasto-plastic finite element analysis. International Journal for Numerical Methods in Engineering 1985;9:149–59.
[5] Polat MU, Dokainish MA. An automatic subincrementation scheme for accurate integration of elasto-plastic constitutive relation. Computers & Structures 1989;31(3):339–47.
[6] Wissmann JW, Hauck C. Efficient elastic–plastic finite element analysis with higher order stress-point algorithms. Computers & Structures 1983;17(1):89–95.
[7] Pezeshk S, Camp CV. An explicit time integration technique for dynamic analysis. International Journal for Numerical Methods in Engineering 1995;38:2265–81.

[8] Sloan SW. Substepping schemes for the numerical integration of elastoplastic stress–strain relations. International Journal for Numerical Methods in Engineering 1987;24:893–911.
[9] Sloan SW, Booker JR. Integration of Tresca and Mohr–Coulomb constitutive relations in plane strain elastoplasticity. International Journal for Numerical Methods in Engineering 1992;33:163–96.
[10] Luccioni LX, Pestana JM, Taylor RL. Finite element implementation of non-linear elastoplastic constitutive laws using local and global explicit algorithms with automatic error control. International Journal for Numerical Methods in Engineering 2001;50:1191–212.
[11] Tamagnini C, Viggiani G, Chamboon R, Desrues J. Evaluation of different strategies for the integration of hyoplastic constitutive equations: application to the CLoE model. Mechanics of Cohesive-Fractional Materials 2000;5:263–89.
[12] Jakobsen KP, Lade PV. Implementation algorithm for a single hardening constitutive model for frictional materials. International Journal for Numerical and Analytical Methods in Geomechanics 2002;26:661–81.
[13] Fellin W, Ostermann A. Consisten tangent operators for constitutive rate equations. International Journal for Numerical and Analytical Methods in Geomechanics 2002;26:1213–33.
[14] Potts DM, Ganendra D. An evaluation of substepping and implicit stress point algorithms. Computer Methods in Applied Mechanics and Engineering 1994;119:341–54.
[15] Gens A, Potts DM. Critical state models in computational goemechanics. Engineering Computations 1988;5:178–97.
[16] Crisfield MA. Non-linear finite element analysis of solids and structures, vol. 1. Basic topics. New York: Wiley; 1997.
[17] Owen DRJ, Hinton E. Finite elements in plasticity: theory and practice. Swansea, UK: Pineridge Press; 1980.
[18] Belytschko T, Liu WK, Moran B. Nonlinear finite elements for continua and structures. New York: Wiley; 1994.
[19] Chen WF. Constitutive equations for engineering materials, vol. 2. Plasticity and modeling. Amsterdam: Elsevier; 2000.
[20] James ML, Smith GM, Wolford JC. Applied numerical methods for digital computation. New York: Harper & Row; 1985.
[21] Dormand JR, Prince PJ. A family of embedded Runge–Kutta formulae. Journal of Computational and Applied Mathematics 1980;6:19C26.
[22] Wallin M, Ristinmaa M. Accurate stress updating algorithm based on constant strain rate assumption. Computer Methods in Applied Mechanics and Engineering 2001;190(42):5583–601.
[23] ABAQUS/Explicit, Version 6.4 manuals. Pawtucket, RI: Hibbitt, Karlsson and Sorensen.
[24] Hill R. A theory of yielding and plastic flow of anisotropic metals. Proceedings of the Royal Society of London Series A 1948;193:281–97.